



Published in final edited form as:

*Nat Biomed Eng.* 2021 September ; 5(9): 1069–1083. doi:10.1038/s41551-021-00780-3.

## Amelioration of post-traumatic osteoarthritis via nanoparticle depots delivering small interfering RNA to damaged cartilage

Sean K. Bedingfield<sup>1</sup>, Juan M. Colazo<sup>1</sup>, Fang Yu<sup>1</sup>, Danielle D. Liu<sup>1</sup>, Meredith A. Jackson<sup>1</sup>, Lauren E. Himmel<sup>2</sup>, Hongsik Cho<sup>3</sup>, Leslie J. Crofford<sup>2,4</sup>, Karen A. Hasty<sup>3</sup>, Craig L. Duvall<sup>1,\*</sup>

<sup>1</sup>Department of Biomedical Engineering, Vanderbilt University, 2301 Vanderbilt Place PMB 351826 Nashville, TN 37235-1826

<sup>2</sup>Department of Pathology, Microbiology and Immunology, Vanderbilt University Medical Center, 1161 21st Ave. South, Suite C-3322 Nashville, Tennessee 37232-2561

<sup>3</sup>Department of Orthopaedic Surgery and Biomedical Engineering, Memphis VA Medical Center, 1211 Union Ave. Suite 520 Memphis, TN 38104

<sup>4</sup>Department of Medicine, Division of Rheumatology and Immunology, Vanderbilt University Medical Center, 1161 21st Ave S, Nashville, TN 37232

### Abstract

The progression of osteoarthritis (OA) is associated with inflammation triggered by the enzymatic degradation of extracellular matrix in injured cartilage. Here, we show that a locally injected depot of nanoparticles functionalized with an antibody targeting collagen type-II and carrying small interfering RNA for matrix metalloproteinase 13 (MMP13), which breaks down collagen type-II, substantially reduced the expression of MMP13 and protected cartilage integrity and overall joint structure in acute and severe mouse models of post-traumatic OA. MMP13 inhibition suppressed clusters of genes associated with tissue restructuring, angiogenesis, innate immune responses and proteolysis. We also show that intra-articular injections of the nanoparticles led to higher reductions in disease progression than either a single injection or weekly injections of the steroid methylprednisolone. Sustained drug retention by targeting collagen in the damaged extracellular

---

Users may view, print, copy, and download text and data-mine the content in such documents, for the purposes of academic research, subject always to the full Conditions of use: <https://www.springernature.com/gp/open-research/policies/accepted-manuscript-terms>

\*Correspondence and requests for materials should be addressed to C.L.D. [craig.duvall@vanderbilt.edu](mailto:craig.duvall@vanderbilt.edu).

#### Author contributions

S.B., C.D., K.H., L.C., and J.C. designed the project and experiments. S.B. synthesized the polymers, conjugates, and formulated nanoparticles for all experiments. S.B. and F.Y. conducted all animal experiments. S.B., M.J., and D.L. performed nanoparticle characterization. S.B., F.Y., J.C., and D.L. imaged and collected tissues. L.H. and H.C. conducted histology and immunohistochemistry with L.H. performing blinded scoring of histology. S.B., C.D., and J.C. wrote the manuscript. All authors reviewed and commented on the manuscript.

#### Competing interests

The authors declare no competing interests.

#### Additional information

**Supplementary information** The online version contains supplementary material available at <https://doi.org/10.1038/s41551-021-00780-3>.

**Peer review information** *Nature Biomedical Engineering* thanks Fergal O'Brien, Ahuva Nissim and the other, anonymous, reviewer(s) for their contribution to the peer review of this work.

**Reprints and permissions information** is available at [www.nature.com/reprints](http://www.nature.com/reprints).

matrix of osteoarthritic cartilage may also be an effective strategy for the treatment of OA with other disease-modifying drugs.

---

Osteoarthritis (OA) is a chronic degenerative disease of the entire joint that leads to pain and loss of mobility, resulting in diminished quality of life. OA is caused by complex interplay between mechanical and biochemical factors<sup>1</sup>. Some well-established risk factors include poor joint alignment or injury<sup>2</sup>, obesity<sup>3</sup>, genetic disposition<sup>4</sup>, and aging<sup>5</sup>. Multiple signaling molecules are known to be central to OA pathogenesis such as interleukin (IL-1 $\beta$ ), Wnt, c-Jun N-terminal kinase (JNK), and reactive oxygen species (ROS)<sup>1,6,7</sup>. All of these signaling pathways independently converge toward increased production of matrix metalloproteinases (MMPs), a step of critical importance in cartilage degradation and progression of OA symptoms<sup>1</sup>.

Post-traumatic osteoarthritis (PTOA) is a form of OA induced by a mechanical joint injury. Common injuries include ligament and meniscal tears, cartilage damage, bone fractures from high impact landings, and dislocations. These injuries are particularly common among young athletes and military personnel and result in an accelerated pathology, requiring surgical intervention 7–9 years earlier on average than standard OA<sup>8</sup>. Though PTOA accounts for only 12% of all OA cases in the United States, it comes at a greater cost and loss of quality adjusted life years (QALYs) due to its earlier and more accelerated onset<sup>9</sup>. PTOA-initiating injuries mechanically disturb the extracellular matrix (ECM) and stimulate synoviocytes and chondrocytes to produce inflammatory cytokines and MMPs<sup>10</sup>. MMPs are key enzymes in OA-related cartilage ECM destruction that degrade the critical structural components of cartilage, including type II collagen (CII). Degradation of CII and other ECM components destroys the chondrocyte niche. Released ECM degradation byproducts also have pro-inflammatory signaling properties<sup>1,11</sup>, triggering a degenerative cycle that perpetuates until the cartilage is fully destroyed. Because patients with joint injuries are highly predisposed to developing PTOA, there is potential for early therapeutic intervention to block disease onset or progression at an early stage.

Current pharmaceutical management of OA is solely palliative, and no disease modifying OA drugs (DMOADs) are clinically approved. There are five FDA-approved corticosteroids for intra-articular OA therapy, but these therapies provide only temporary pain relief. Steroids do not target the underlying cause of disease and are not recommended for long-term management<sup>12</sup>, as they have been shown to actually cause cartilage volume loss (when given 4 times per year for 2 years)<sup>13</sup>, have been shown to increase the risk of requiring joint replacement<sup>14</sup>, and have associations with chondrotoxicity<sup>15</sup>. MMP13 is a key proteolytic driver of cartilage loss in OA, as indicated by reduced surgically-induced OA progression in MMP13 knockout mice and in wild type mice treated with broad MMP inhibitors<sup>16</sup>. Unfortunately, clinical trials on MMP small molecules inhibitors (tested mostly for cancer treatment) have been suspended due to pain associated with musculoskeletal syndrome (MSS). Patient MSS is believed to be linked to systemic delivery of small molecules that non-selectively inhibit multiple MMPs, some of which (MMP2, 3, 4, 7 and 9) are involved in normal tissue homeostasis<sup>17–19</sup>. Production of selective small molecule inhibitors is complicated by shared domains of the collagenases and the homology of the catalytic site

<sup>20</sup>. One tested MMP13 inhibitor PF152 reduced lesion severity in a canine PTOA model <sup>21</sup> but unfortunately caused nephrotoxicity, likely through off-target effects on the human organic anion transporter 3 <sup>22</sup>. For these reasons, we hypothesize that selectively targeting MMP13 (which has not been associated with MSS) through delivery of a locally-retained RNA interference (RNAi) therapy could be an effective and safe approach for blocking the degenerative PTOA process following joint injury.

Intraarticular injections are clinically-utilized in OA, yet face unique drug delivery challenges. One of the major barriers is that synovial fluid is continuously exchanged in the joint, causing most drugs to be rapidly cleared into the lymphatic system <sup>23,24</sup>. The synovial vasculature clears small molecules, while the lymphatics drain away macromolecules <sup>25,26</sup>, resulting in joint half-lives ranging 1–4 hours for commonly used steroids <sup>24</sup>. These challenges leave an unmet need for OA therapies that are better retained within the joint after local injection. Targeting of nanoscale particles is one promising approach that has traditionally relied on using chondroitin sulfate, CII-binding peptides, and bisphosphonates <sup>27–29</sup>. Chondroitin sulfate and CII-binding peptides anchor particles to the cartilage matrix and reduce convective transport through synovial fluid flow, while the bisphosphonates can be used to bind to subchondral bone which can be exposed in advanced OA disease. ECM bioadhesion has been minimally utilized for delivery of small molecules and has not been investigated, to our knowledge, for local retention of biologics with intracellular targets <sup>30</sup>.

Here, we sought to anchor MMP13 RNAi nanoparticles to sites of early cartilage damage in OA and to confirm that matrix targeting can provide functional benefit for delivery of intracellular-acting biologics. RNAi is critical in this application because siRNA can be designed to have selective complementarity with MMP13 mRNA, obviating the enzyme selectivity concerns associated with small molecule inhibitors. The clinical utility of siRNA medicines is supported by the recent clinical trial success and FDA approval of both Alnylam's ONPATTRO™ (patisiran) for treatment of hereditary transthyretin-mediated amyloidosis and GIVLAARI™ (givosiran) for acute hepatic porphyria <sup>31,32</sup>. Here, we extended polymeric siRNA nanopolyplexes (siNPs) recently developed by our research group <sup>33–36</sup> to develop a form of this carrier that binds to sites of early OA cartilage damage using a collagen type 2 monoclonal antibody (mAbCII, E4-D4 clone, Supplementary Fig. 1). The mAbCII clone utilized recognizes an epitope of cyanogen bromide peptide 10 and has been proven to be cross-reactive with CII from multiple species (mouse, human, porcine, bovine, guinea pig) but not type 1 collagen. The antibody epitope becomes more accessible when other proteins or proteoglycans in the cartilage matrix are lost. Previous studies show that cartilage CII is more exposed and accessible for binding after injury <sup>37</sup> and that the mAbCII antibody can be used as a targeted nano-diagnostic for intravitality measuring severity of OA <sup>38</sup>. In the current report, we formulated and therapeutically tested mAbCII-functionalized siNPs (mAbCII-siNPs) as a locally-injectable system that creates an *in situ* depot of MMP13 RNAi nanomedicine in PTOA-afflicted joints. Matrix-targeted delivery of an intracellular-acting biologic such as siRNA represents a significant departure from the convention of targeting internalizing cellular receptors. Herein, we validate the utility of this approach and prove it therapeutically significant as a DMOAD in a model of mechanical PTOA.

## Results and discussion

The mAbCII-siNPs were synthesized comprising an endosome-escaping, RNA-condensing core and a passivating, colloiddally-stabilizing poly (ethylene glycol) (PEG) surface amenable to antibody conjugation (Fig. 1a). The diblock copolymer that constitutes the siNPs was synthesized through reversible addition-fragmentation chain transfer (RAFT) polymerization of a random copolymer of 50 mol% 2-(dimethylamino)ethyl methacrylate (DMAEMA) and 50 mol% butyl methacrylate (BMA) from a carboxy-PEG-ECT (4-cyano-4 (ethylsulfanylthiocarbonyl) sulfanylpentanoic acid) macro-chain transfer agent (macro-CTA) and verified by NMR (Supplementary Fig. 2). The poly(DMAEMA-co-BMA) (DB) random copolymer block has a balance of hydrophobic BMA and cationic DMAEMA monomers that has been finely tuned to drive NP self-assembly and stabilization (BMA), enable electrostatic siRNA packaging (DMAEMA), and have an appropriate  $pK_a$  and level of hydrophobicity that drives pH-dependent membrane disruptive function in the early endosomal pH range<sup>39–42</sup>. The collagen II targeting mAbCII was conjugated to COOH-PEG-ECT by N-hydroxysulfosuccinimide; 1-Ethyl-3-(3-(dimethylamino)propyl) carbodiimide (sNHS/EDC) chemistry (Fig. 1b). Successful conjugation of PEG-*b*-DB to mAbCII was validated by fast protein liquid chromatography (FPLC; Supplementary Fig. 1d), and the resultant polymers were formulated into siNPs by complexation with siRNA at pH 4 followed by raising to physiologic pH (Fig. 1c). The control groups included bare-siNPs (no antibody conjugation) and siNPs functionalized with a control off-target antibody (mAbCtrl siNPs). “Dual hydrophobization” was also employed in all siNP formulations. This approach combines the hydrophobicity of BMA in the core of the siNP with C16 modification of the siRNA through conjugation to palmitic acid in order to improve siNP stability and gene silencing longevity of action<sup>35,43</sup>.

### Chemicoophysical, In Vitro Characterization of mAbCII-siNPs.

The underlying siNP that was developed here in a mAbCII-functionalized format has been previously characterized by our group<sup>33,40,43,44</sup>. These studies have consistently shown a hydrodynamic diameter of ~100 nm and approximately neutral zeta potential due to the PEG (or in some formats zwitterionic siNP surface forming polymer block). The *in vivo* circulation half-life after intravenous injection is ~20 minutes<sup>33</sup>. These siNPs are cytocompatible *in vitro*<sup>33</sup> and can be tolerated upon repeated, intravenous administration *in vivo*, with minimal histologic or immunologic consequences<sup>43</sup>.

The hydrodynamic diameter, siRNA encapsulation efficiency, pH-dependent membrane disruptive behavior (as an indirect indicator of endosome escape), and cell viability were assayed for mAbCII-siNPs compared to non-targeted siNPs. The mAbCII-siNPs were not statistically different from the non-functionalized siNPs in all these assays (Fig. 2a–d). The mAbCII-siNPs, prepared at a 1:40 antibody:polymer ratio for optimized cartilage binding (Fig. 2f), had an average hydrodynamic diameter of 124 nm with a PDI of 1.1 as determined by dynamic light scattering (Fig. 2a). Encapsulation of siRNA was efficient (~80%) at  $N^+ : P^-$  ratios (ratio of positive nitrogen groups,  $N^+$ , in polymer side chains to negative phosphodiester groups,  $P^-$ , in the siRNA backbone) of 10 or above (Fig. 2b). The hemolysis assay demonstrated significant membrane lysis at the early endosome pH (6.8) and below

and negligible activity at extracellular pH (7.4) (Fig. 2c). Cell viability was approximately 80% or greater for doses of 150 nM or less (Fig. 2d).

Silencing of MMP13 was tested in cultured, chondrogenic ATDC5 cells stimulated with TNF $\alpha$ . The cells were pretreated for 24 h with the siRNA formulations, stimulated with 20 ng mL<sup>-1</sup> TNF $\alpha$  for 24 h, and then assayed for MMP13 gene expression using TaqMan PCR. Information on screens that identified the leading MMP13 siRNA sequence are found in Supplementary Table 1 and Supplementary Fig. 2. The best candidate (siMMP13) demonstrated greater than 80% knockdown with a 50 nM dose delivered by the mAbCII-siNPs when compared with a nontargeting siRNA sequence (siNEG) (Fig. 2e). These data show that siNP bioactivity is maintained following antibody conjugation and that the mAbCII-siNPs can achieve potent MMP13 silencing in cells under pro-inflammatory conditions.

### **Ex vivo CII targeting, substrate-mediated RNAi in ATDC5 cells.**

The mAbCII-siNPs were assessed for binding to porcine cartilage explants that were pre-treated with trypsin, which initiates formation of lesions of the articular surface, similar to what is seen in OA<sup>45</sup>. Trypsin does not damage the triple helical structure of type II collagen but rather removes the telopeptide ends of the monomer and does not remove the native epitope; unless the collagen is newly synthesized, non-enzymatic cross-links formed over time maintain the monomer in the fibrillar structure upon trypsin exposure. Trypsin pre-treatment was used in the screening model to mimic OA damage and because the mAbCII antibody preferentially binds to CII that becomes accessible when cartilage is mechanically or proteolytically damaged<sup>46,47</sup>. The mAbCII-siNPs were prepared with a range from 20:1 to 80:1 non-conjugated polymer: antibody modified polymer molar ratios. The polymers used comprised rhodamine acrylate (exc/emm: 548/570 nm) copolymerized at 1 mol% in the poly(DMAEMA-co-BMA) block to enable fluorescent measurement of carrier retention on the damaged cartilage plugs. Retention of siNPs on trypsin-damaged cartilage after washing with phosphate buffer saline (PBS) was quantified by IVIS imaging and showed that conjugation of mAbCII to the polymer at 40:1 polymer:mAbCII molar ratio provided the best retention performance (Fig. 2f; Supplementary Fig. 4a). These data confirm that mAbCII conjugation enhances binding of siNPs to exposed CII in damaged cartilage and motivated our focus on the 40:1 conjugation ratio for subsequent studies. The optimized mAbCII-siNP formulation was also confirmed to preferentially bind to trypsin damaged over undamaged cartilage plugs (Fig. 2g).

Subsequently, the porcine cartilage binding assay was adapted to confirm whether matrix bound mAbCII-siNPs could achieve effective substrate-mediated siRNA delivery and bioactivity. Following incubation of all siNP groups loaded with anti-luciferase siRNA (siLuciferase) with trypsin-damaged cartilage, a PBS washing step was done to simulate synovial fluid clearance. Murine chondrogenic ATDC5 cells that were lentivirally transduced in-house with a constitutive luciferase reporter were then seeded over the damaged cartilage that had been pre-treated with mAbCII-siNPs, bare-siNPs, mAbCtrl-siNPs. In parallel, the same groups were run without the washing step to experimentally dissect the benefit of siNP matrix binding and retention. Significantly higher luciferase

silencing was observed with mAbCII-siNPs compared to bare-siNPs and mAbCtrl-siNPs when a wash step was used prior to cell seeding (Fig. 2h). Following the measurement of luciferase expression, cell viability of each group was determined using the Promega CellTiter-Glo luminescent cell viability assay following Promega's standard protocol. These data confirm a potential pharmacokinetic benefit of siNP matrix binding and that substrate-mediated delivery of matrix-targeted siNPs achieves target gene silencing.

### ***In vivo* CII-anchoring-dependent MMP13 silencing.**

An acute PTOA model of noninvasive repetitive joint loading was used by subjecting the left knee of 8-week-old C57BL/6 mice to 500 cycles of compressive mechanical loading at 9N (Fig. 3a). This procedure was repeated three times per week over a period of two weeks using conditions adapted from previous studies<sup>38,48</sup>. Following loading, mice were treated via intraarticular injection of 0.5 mg/kg per knee of formulated siRNA with mAbCII-siNPs, bare-siNPs, or mAbCtrl-siNPs. All forms of siNPs contained a rhodamine acrylate monomer integrated into the poly(DMAEMA-*co*-BMA) block that forms the NP core, enabling IVIS fluorescence imaging to assess pharmacokinetics.

To compare *in vivo* retention of mAbCII-siNPs between healthy (unloaded) and PTOA (loaded) knees, explanted knees were imaged at 72 h after injection (Fig. 3b), revealing that mAbCII-siNPs were preferentially retained in PTOA over non-injured knees (Fig. 3c). The mAbCII-siNPs also had significantly higher retention within PTOA joints compared to mAbCtrl- and bare-siNPs (Fig. 3d–g; Supplementary Fig. 4b). Biodistribution to the major clearance organs including liver, kidney, spleen was also measured by IVIS imaging. The mAbCII-siNP retention in the PTOA knee reduced the biodistribution to the liver versus animals without PTOA that were intra-articularly injected with mAbCII-siNPs (Supplementary Fig. 5a,b). To confirm whether mAbCII-siNPs achieved cartilage penetration and delivery to the chondrocytes, cryosections were imaged from knees explanted 12 hours after intra-articular injection (Fig. 2g). mAbCII-siNPs can be visualized at the articular cartilage surface and are also seen concentrated in individual chondrocytes (orange signal), meanwhile mAbCtrl-siNPs showed some signal at the articular cartilage surface, but did not show evidence of retention within the chondrocyte niche. The observation of localization both to the articular surface and to the chondrocyte niche are consistent with that previously seen for CII-targeting peptide-functionalized nanoparticles<sup>27</sup>.

Gene silencing activity *in vivo* in PTOA-affected joints was next compared for mAbCII-siNPs and control formulations injected using the same 2-week mechanical loading protocol. Gene expression analysis on joints harvested 3-days after intra-articular treatment confirmed that the ECM anchoring of the mAbCII-siNPs enabled more potent MMP13 expression silencing relative to bare- or mAbCtrl-siNPs. The mAbCII-siNPs achieved greater than 90% target gene knockdown in the mechanically-loaded PTOA joints (Fig. 2h). Dose dependent *in vivo* gene silencing activity of mAbCII-siNPs was also measured for 0.125, 0.25, and 0.5 mg/kg siMMP13 relative to siNEG (0.5 mg/kg) in PTOA knees. At 72 h post-treatment, total MMP activity was quantified by IVIS imaging 24 h after intravenous injection with MMPsense (probe activated by MMPs 2, 3, 7, 9, 12, and 13), showing that 0.25 and

0.5 mg/kg siMMP13 doses delivered with mAbCII-siNPs significantly reduced total MMP activity (Fig. 2 i,j). MMP13 and IL-1 $\beta$  expression were quantified in the same experiment by TaqMan qPCR from joint samples collected at 72 h following treatment (Supplementary Fig. 6a,b), motivating our use of a 0.5 mg/kg per knee dose for subsequent, longer-term studies designed to assess mAbCII-siNPs/siMMP13 therapeutic efficacy as a DMOAD. Longevity of silencing was also assayed at the 0.5 mg/kg dose (Supplementary Fig. 5e), motivating use of a weekly dose in subsequent studies.

### **MMP13 silencing in longer-term osteoarthritis mouse model.**

A 6-week murine study was completed to evaluate the therapeutic effect of weekly doses of MMP13-silencing mAbCII-siNPs in a longer-term and more aggressive PTOA model. Tests for the more aggressive PTOA model were carried out in C56BL/6 mice aged to 6 months and subjected to a more rigorous cyclic mechanical loading protocol of 9N, 500 cycles, 5 times per week, for 6 weeks (Fig. 4a)<sup>49</sup>. Doses of 0.5 mg/kg siRNA were administered into each knee weekly, starting concurrently with mechanical loading. MMPsense and Alexafluor-labeled mAbCII antibody were injected intravenously 24 h before sacrifice to gauge total MMP activity and quantify cartilage damage, respectively. Even though the study takedown and gene expression analysis were done a full week following administration of the final dose, MMP13 expression interference achieved with mAbCII-siNPs was consistent with the short-term model, with greater than 80% reduction compared to OA joints treated with siNEG using mAbCII-siNPs (Fig. 4b). Immunohistochemical (IHC) staining revealed that MMP13 production both in the articular cartilage and the synovial tissue was reduced by mAbCII-siNP/siMMP13 treatment (Fig. 4c,d). The inflammation associated with PTOA is characterized by detrimental tissue restructuring potentiated by cytokines and growth factors produced in the synovium of the joint<sup>50</sup>. Degradation products of degraded CII have signaling properties that contribute to catabolic activity, hypertrophy, and apoptosis<sup>51</sup>. The mAbCII-based retention of siMMP13 in the PTOA joint provide both primary, cartilage-protective effects and also secondary effects associated with reduced production of degradation products that signal for downstream production of inflammatory cytokines and MMPs by the synovium.

Histological analysis showed that mAbCII-siNP/siMMP13 treatment significantly reduced PTOA-associated joint structural changes. Coronal sections of fixed knee joints were stained with Safranin O and Fast Green to evaluate cartilage histopathology (Fig. 4e; Supplementary Fig. 7). Sections were then blindly scored by a trained pathologist using the criteria outlined in Supplementary Table 2a,b. Safranin O stains proteoglycans associated with normal cartilage a deep red and is used for histopathological scoring of cartilage as recommended by the Osteoarthritis Research Society International (OARSI)<sup>52</sup>. The reduced Safranin O staining and surface discontinuity observed in untreated OA and siNEG-treated OA is indicative of proteoglycan loss and cartilage erosion and was significantly prevented in siMMP13-treated joints, as reflected in the disparate OARSI scores between treatment groups (Fig. 4f).

Total MMP activity was also significantly reduced in the mAbCII-siNP treated animals compared to controls that were either untreated or treated with mAbCII-siNPs loaded with

siNEG (Fig. 4g). Relative binding of Alexafluor-labeled mAbCII antibody to pathologically exposed CII is a biomarker for degree of cartilage damage<sup>38,53,54</sup> and was thus used here as an intravital readout for disease severity. Significantly greater binding of mAbCII was observed in mAbCII-siNP/siNEG treated and untreated mice compared to mAbCII-siNP/siMMP13 treated mice, indicating that MMP13 silencing protected the cartilage structure (Fig. 4h,i). Levels of Alexafluor680-mAbCII binding in the PTOA joint were similar between untreated mice and mAb-CII-siNP/siNEG treated mice, indicating that treatment with mAbCII-functionalized siNPs one week prior did not in itself interfere with the subsequent mAbCII-based cartilage damage measurement.

Hematoxylin and eosin (H&E) staining was used to evaluate overall joint status, including response in the meniscus and synovium (Fig. 5a; Supplementary Fig. 8). Joint mechanical loading induced robust synovial thickening, osteophytes, and mineralization in the meniscus. Whole joint histology was blindly scored by a pathologist (Fig. 5b) based on the degenerative joint disease criteria outlined in the supplemental information (Supplementary Item #1, Table S2). While cartilage structure was strongly protected by mAbCII-siNP/siMMP13 treatment (treated mice did not have statistically different OARSI score compared to normal mice with no load-induced PTOA), it also better preserved the normal structure of the synovium and meniscus compared to control-treated animals. The H&E joint sections for siNEG and untreated groups consistently had more synovial hyperplasia, larger osteophytes, and more mineralization in the menisci compared to the mAbCII-siNP/siMMP13 group. Use of micro computed tomography (microCT) to more globally visualize and quantify ectopic mineralization revealed that mAbCII-siNP/siMMP13 treatment significantly protected against meniscal mineralization and osteophyte formation (Fig. 5c–g; Supplementary Fig. 9a). These data support that MMP13 silencing provides secondary benefits to the joint in addition to directly reducing articular cartilage loss.

When evaluating OA joints clinically, the presence of osteophytes and ossified nodules within the meniscus and synovium is especially important, as these characteristics are used to gauge OA progression and appear in the most advanced stages of the disease<sup>55,56</sup>. These rigid calcium deposits are associated with synovial macrophage activation in experimental OA<sup>57</sup> where they concentrate local mechanical stress. Further, presence of calcium phosphate can exacerbate synovitis by activating inflammasomes and consequently triggering production of the OA driver IL-1 $\beta$ <sup>58</sup>. While inflammation affects patient comfort, complications and acute pain from osteophytes and calcium deposits are often cited as primary reasons for advanced OA patients to resort to total knee replacement<sup>59</sup>. Inhibiting pathological ossification would be anticipated to enable maintenance of an active lifestyle and to delay total knee replacement.

To look more broadly at the joint and surrounding tissues, subchondral trabecular bone was also characterized using microCT. Interestingly, mAbCII-siNP/siMMP13 treatment significantly reduced loss of subchondral trabecular bone volume associated with PTOA (Supplementary Fig. 9b). TRAP (tartrate-resistant acid phosphatase) staining was also performed to assess osteoclast activity as a snapshot of bone resorption (Supplementary Fig. 9c). Activated osteoclasts were increased in untreated, mechanically loaded knees compared to those receiving mAbCII-siNP/siMMP13 treatment. These data reinforce the complexity

of OA as a full joint disease, while also indicating that MMP13 RNAi has beneficial, global impacts within the joint by also impacting cartilage crosstalk with surrounding tissue. There is strong clinical precedent for observing multiple, concomitant types of aberrant mineral homeostasis within the OA joint. Clinically, calcium deposits often manifest in the meniscal and synovial tissue and fluid. At the same time, pathological vascularization and thickening of the subchondral bone plate can cause loss of subchondral trabecular bone<sup>58</sup>. Animal models and human samples suggest an influence of MMP13 and cathepsin K, specifically, in driving pathological subchondral bone resorption in late-stage OA in human tissues<sup>60</sup>. In accordance with these studies, we find that subchondral bone resorption and pathologic bone restructuring within the whole joint are reduced with MMP13 inhibition.

The rigorous model used in this study induced several aspects of joint pathology observed clinically including articular cartilage loss, soft tissue mineralization, osteophyte formation, and remodeling of subchondral bone. This model is based on repeated mechanical loading of the joint in flexion rather than a single surgical or injury procedure that induces a torn/transected ligament, as is commonly done for modeling PTOA. The repeat mechanical loading model has been validated in previous publications<sup>48</sup>. One benefit of this model is that it does not require an invasive surgical procedure that can, in of itself, damage the joint. Also, we find a more consistent phenotype and less variability than with surgical models because the joint injury is created by the cumulative effect of multiple loading sessions over time using a highly-controlled mechanical testing apparatus. Importantly, the repeated mechanical loading model reproduces many of the characteristics of other preclinical models of PTOA and of clinical PTOA, including cartilage deterioration, heterotopic ossification, and inflammation<sup>61</sup>. The model that we used here is also comparable to a related load-induced PTOA model that uses mechanical loading to tear the anterior cruciate ligament (ACL;<sup>62</sup>. The overload-induced ACL tear model is characterized by significant joint structural changes with osteophytes forming on the anteromedial aspect of the distal femur and the posteromedial aspect of the proximal tibia, in addition to ectopic mineralization occurring in the medial meniscus<sup>62</sup>, analogous to the joint effects seen in our studies (Figs 5 and 6). It will be of significant interest to ultimately test this experimental therapy in larger animal models in which joint dimensions and OA pathogenesis more accurately resembles humans.

### **MMP13 silencing broadly affects OA-associated gene expression.**

Targeting MMP13 directly by RNAi silenced MMP13 and was found to have broad effects on overall joint health, including both the articular cartilage and surrounding hard and soft tissues. To further characterize the global impacts of targeted MMP13 inhibition, the mechanical loading mouse model was repeated with the same parameters except that samples were harvested at 4 rather than 6 weeks to capture a more intermediate stage of disease (Fig. 6a). The nanoString nCounter Inflammation panel was used to quantify expression of 254 genes in the knee joint samples (articular cartilage, meniscal, and synovial tissue). Unsupervised analysis using nanoString software indicated that the joints treated with mAbCII-siNPs/siMMP13 were closer to normal tissue and more different from untreated OA tissue than mAbCII-siNPs/siNEG (Fig. 6b). Compared to treatment with mAbCII-siNPs/siNEG, treatment with mAbCII-siNPs/siMMP13 significantly suppressed

expression levels of several clusters of genes with notable associations with OA progression (Fig. 6c,d).

In PTOA joints, mAbCII-siNPs/siMMP13 treatment significantly reduced clusters of genes associated with tissue restructuring and angiogenesis. Tissue remodeling is an active process in response to injury, in the articular cartilage and especially in the synovium where capsule thickening, vascularization, and hyperplasia occurs. These processes are associated with the upregulation of genes such as MEF2 $\alpha$  (chondrocyte hypertrophy) and PDGF $\alpha$  (a potent synovial fibroblast growth factor)<sup>63,64</sup>, which were suppressed by mAbCII-siNPs/siMMP13. MMP13 silencing also suppressed Flt-1, which is a VEGF receptor, predominantly expressed by vascular endothelial cells and involved in angiogenesis. The less active tissue remodeling and thickening processes in mAbCII-siNP/siMMP13 treated joints was also associated with suppression of gene clusters related to proteolysis and skeletal development. MMP13 silencing also led to downregulation of genes associated with apoptosis, such as Jun (which also induces MMP13) and the inflammatory cytokine IL6, which is mechanistically involved in propagation of cellular stress and synovial inflammation<sup>65,66</sup>.

Treatment-associated downregulation of genes related to tissue restructuring, apoptosis, angiogenesis, and proteolysis were also complemented by reduction of innate immune activation in joints with targeted MMP13 silencing. PTGS2 (prostaglandin-endoperoxide synthase 2), an inflammation driver that encodes the cyclooxygenase 2 enzyme (COX2) was significantly reduced in mechanically loaded joints with mAbCII-siNP delivery of siMMP13 versus siNEG. Treatment also suppressed expression of IL1RN, which encodes the interleukin 1 receptor antagonist protein (IL1RaP); knock-out of this gene correlates with spontaneous arthritis development<sup>67</sup>. Coupled with reduction of innate immune response, MMP13 silencing also reduced expression of several serine proteases (C1S, C1RA, and C2) that are components of the complement pathway, which is known to be associated with OA progression<sup>68,69</sup>. This suggests that there is less local influx or activation of circulating monocytes, macrophages, and monocyte-derived dendritic cells that express C1s, C1RA, and C2<sup>70</sup>. MMP13 silencing also reduced expression of IL-1 $\beta$  (MAPK activation cluster), an inflammatory cytokine that drives OA by inducing nitric oxide production, increasing synthesis of MMPs and aggrecanases, and suppressing proteoglycan synthesis<sup>71</sup>. Interestingly, recent work has highlighted that macrophages present in synovial tissue can induce a proinflammatory state<sup>72</sup> and that these cells, in combination with synovial fibroblasts, are primary contributors to MMP13 expression within the joint. MMP13 inhibition directly reduces cartilage degradation, but these larger-scale changes in tissue gene expression further support that this treatment impacts overall joint health; these broader joint effects may be at least partially due to disrupting the “degenerative cycle” that is perpetuated by degradative products of the cartilage matrix<sup>16</sup>.

The global changes to inflammatory gene expression observed in this study, in combination with joint analysis utilizing microCT and histology, all support the therapeutic value and safety of local, MMP13 RNAi nanomedicine that anchors to the cartilage ECM. It is thought that MMP13 activity within the synovial joint drives OA progression<sup>73</sup>. By contrast, MMP13 expression by osteocytes is important for normal perilacunar/canalicular

remodeling (PLR). Selective genetic ablation of MMP13 expression in osteocytes disrupts subchondral bone homeostasis in a way that exacerbates subchondral bone sclerosis and OA pathology<sup>74</sup>. However, the OA phenotype in these mice was also associated with a compensatory upregulation of MMP13 expression by the chondrocytes. In light of this observation, the significance of MMP13 inhibition in osteocytes on OA remains an open question. We speculate that a CII-targeted delivery system such as mAbCII-siNPs that is injected directly into the intraarticular space will localize effects to cartilage and adjacent synovial tissues, while any unbound treatment would clear primarily through lymphatic drainage<sup>75</sup>, limiting exposure and gene targeting effects on cells embedded within the more remote bone. MicroCT analyses showed that mAbCII-siNP/siMMP13 treatment maintained a more normal subchondral bone volume fraction and reduced both osteophytes and ectopic mineralization, suggesting that matrix-tethering siNPs actually normalized mineralization homeostasis within the joint. This matrix-anchoring system may enable a desirable combination of safe and effective therapeutic MMP13 targeting that may be difficult to achieve with systemic delivery or through delivery of small molecule inhibitors that more readily diffuse into surrounding tissues.

### **Benchmark comparisons to clinical standard steroid treatment.**

After broadly characterizing the joint structural and gene expression implications of mAbCII-siNPs/siMMP13, benchmarking was done against a current standard therapy using the 6-week study protocol. The most prevalent clinical intervention beyond the use of oral NSAIDs is the intraarticular administration of steroids, which are recommended to be given up to four times per year<sup>76</sup>. The most commonly used corticosteroid is methylprednisolone<sup>77</sup>. Because the longer-term, 6-week osteoarthritis mouse model used in our therapeutic studies is aggressive, testing was done for both a single dose of methylprednisolone at the time of first injury (most similar to frequency of dosing used clinically) and a weekly dose, with the latter done to match the protocol used for testing of mAbCII-siNPs/siMMP13 (dosing described further in Supplemental Information).

Histological sections of the joints from the steroid treatment study were blindly scored by a pathologist following tissue staining with hemotoxylin/eosin and safranin-O (Fig. 7a–d). Neither single or weekly methylprednisolone injections significantly altered either the OARSI or Degenerative Joint Disease Scores relative to untreated PTOA knees. These findings are in agreement with other studies demonstrating that while steroids temporarily alleviate inflammatory pain, there is no demonstrated protection of cartilage structural integrity<sup>12</sup>. Notably, mAbCII-siNPs/siMMP13 treatment significantly reduced both the DJD and the OARSI score relative to controls, while neither single nor weekly steroid treatment provided any significant protection by these joint scoring metrics. Like the histological scoring outcomes, neither steroid treatment protocol blocked osteophyte formation or ectopic mineralization, unlike mAbCII-siNP/siMMP13 therapy (Fig. 7e). These distinctions further highlight the therapeutic potential of specific inhibition of MMP13, a molecular driver that broadly underlies several aspects of PTOA joint destruction.

## Outlook

RNAi silencing of MMP13 using matrix-anchoring nanocarriers to prolong retention within the osteoarthritic joint provides significant therapeutic benefit in blocking PTOA progression. This study validates the unique concept that matrix binding for local retention of an in situ formed nanoparticle-based depot is a viable strategy to improve potency and longevity of action of intracellular biologics such as siRNAs. While formulation of larger sized (micro-scale) particles may also facilitate retention, it would not be anticipated to be effective for intracellular acting drugs because of endocytosis, endosome escape, and tissue penetration limitations of larger particles<sup>78</sup>. The current system, which uses antibody targeting to reduce joint clearance, achieved as high as 90% target gene silencing in vivo with gene silencing remaining potent even 1 week after the final treatment in a 6-week study. Furthermore, local retention of the injected dose and specific targeting of MMP13 are anticipated to reduce the toxicity concerns that have become associated with systemically-delivered, non-selective synthetic small molecule MMP inhibitors. The therapeutic relevance of this approach is exemplified in an aggressive, long-term PTOA model which showed a treatment-associated 80% reduction in MMP13 expression, protection of cartilage integrity, improvement in total joint histopathology, reduced ectopic mineralization and osteophyte formation, and less destruction of subchondral bone. None of these beneficial effects were seen with corticosteroid treatment, the clinical standard for OA palliation.

## Methods

### mAbCII Antibody.

Monoclonal antibody (E4-D4 clone) to purified bovine type II collagen was prepared from a hybridoma clone isolated as previously described<sup>79</sup>. CNBr-derived peptides were obtained by cyanogen bromide cleavage of denatured bovine type II collagen, and the unpurified peptides were separated by PAGE and immunoblotted against the E4-D4 clone.

The clones were characterized by ELISA against native type II collagens prepared from mouse, pig, bovine, and human cartilage and by Western blot analyses against intact and CNBr-derived peptides of bovine type II cartilage (Supplementary Fig. 1a–c).

### Synthesis and conjugation of polymers.

The synthesis scheme (Fig. 1) was followed as described in the manuscript, utilizing RAFT polymerization with incremental steps verified by NMR. *N*-hydroxysuccinimide-functionalized 4-cyano-4 (ethylsulfanylthiocarbonyl) sulfanylpentanoic acid (NHS-ECT) synthesis was verified by NMR (Supplementary Fig. 2a), and the product was then conjugated to an amine-carboxy heterobifunctional 5kD PEG to form carboxy-PEG-conjugated ECT for use as an initial chain transfer agent for RAFT polymerization<sup>39</sup>. A co-polymer of DMAEMA (2-(Dimethylamino)ethyl methacrylate) and BMA (butyl methacrylate) was chain extended from the COOH-PEG-ECT with a desired target degree of polymerization of 150 (1:1 molar ratio DMAEMA:BMA) to create PEG-DB which was verified by NMR (Supplementary Fig. 2b). The reaction was purged with nitrogen for 30 minutes. AIBN was utilized as an initiator (10:1 CTA:Initiator ratio) in 10% w/v dioxane.

The reaction was stirred at 65 °C for 24 h before precipitation into ether and vacuum drying for 24 h. Polymer was then dissolved and dialyzed in methanol for 48 hours before transition to dialysis in water for another 48 hours.

Subsequently, a two-stage sulfoNHS/EDC conjugation protocol was optimized for activating the polymer and removing excess activating compounds before mixing of the polymer with the antibody to avoid antibody crosslinking. Carboxyl terminated PEG-DB polymer was dissolved in ethanol at a 20 mg/mL concentration before addition to 0.05 M MES buffer, pH=6.0 to prepare a final 1 mg/mL solution of COOH-PEG-DB polymer. EDC and sNHS were added at 250 and 500 mM and allowed to react for 15 minutes at room temperature. Excess EDC and sNHS were then eliminated using 10kD MWCO spin filters from Amicon, centrifuging at 3,000 rcf for 13 minutes from an initial volume of 6 mL. The total volume was then reconstituted to 6 mL by addition of more MES buffer. Antibody at 1 mg/mL in 0.1M PBS, pH=8.0 was added to the activated polymer solution and allowed to react for 18 h at room temperature. Conjugation was verified by size exclusion chromatography as shown in Supplementary Fig. 1d, tracking polymer elution by absorbance at 214 nm through Enrich SEC 650 columns at a flow rate of 0.25 mL/min in 10 mM PBS at pH 8. In the final siNP formulation, antibody-conjugated mAbCII-PEG-DB was mixed with non-functionalized PEG-DB at defined ratios (usually 1:40 conjugated to nonfunctionalized polymer).

#### **Formation of mAbCII-siNPs.**

Polyplexes were formed by dissolving polymers in 10 mM citric acid buffer (pH 4) before complexation with siRNA for 30 minutes. Polymer was initially dissolved at 3 mg/mL concentration. The siRNA (palmitic acid-modified siRNA) was complexed at the N:P ratio of 20. Following complexation, the pH was neutralized to 7.4 with sodium phosphate buffer (10 mM; pH 8; 5:1 v/v ratio).

For *in vivo* experiments, siNPs were formed under the same conditions and concentrated using 50kD MWCO 15 mL Amicon spin filters, washing with PBS, and sterile-filtered before injection.

#### **Characterization of particles (siNPs).**

The mAbCII-siNPs were characterized to verify that the si-NP functionality was not compromised by antibody conjugation. The efficiency of siRNA encapsulation N<sup>+</sup>:P<sup>-</sup> ratios was evaluated using a Quant-iT Ribogreen assay kit (ThermoFisher Scientific, Waltham, MA). siNP size was evaluated using dynamic light scattering (DLS) (Zetasizer Nano ZS, Malvern, USA). Polymer pH-dependent membrane disruptive function as a marker for endosome disruption/escape was evaluated using a hemolysis assay, as described previously<sup>80</sup>.

#### **Selection of MMP13 siRNA.**

Seven candidate siRNA sequences targeting different sites of the MMP13 gene were first screened in ATDC5 cells stimulated with the inflammatory cytokine TNF $\alpha$  (20 ng/mL). Oligonucleotides used in these studies were purchased from Integrated DNA Technologies

(Coralville, IA, USA) or Dharmacon, Incorporated (Lafayette, CO, USA). The selected sequence was synthesized with 2' *O*-methyl modification for enhanced *in vivo* activity (Table S1).

### Cell culture and viability studies.

ATDC5 cells were cultured in DMEM / F-12, GlutaMAX medium with 10% FBS, 1% penicillin/streptomycin at 37 °C in 5% carbon dioxide. Relevant experiments were performed at 80% confluency. Cytotoxicity was performed using the CellTiter-Glo assay, in accordance with the manufacturer's protocol.

### Luciferase gene silencing assay.

For *in vitro* luciferase knockdown assays, ATDC5 cells were lentivirally transduced with constitutively-expressed luciferase gene in a manner previously described<sup>36</sup>. Cells were then seeded at 2,000 per well in clear-bottom, black-walled 96-well plates. After allowing cells to adhere for 24 hours, siNPs were then introduced into cell media at a concentration of 100 nM siRNA (siLUC or siNEG). Treatments were removed after 24 hours of incubation, D-Luciferin (150 µg/mL) was added onto the cells, and cell bioluminescence was then measured on an IVIS Lumina III imaging system (Caliper Life Sciences, Hopkinton, MA) at 24 and 48 hours after treatment. Luminescence was normalized to that of siNEG NP controls. Finally, cell viability was measured by comparing luminescence of siNEG controls to untreated cells.

### Quantitative reverse transcription PCR.

Real-time qRT-PCR was performed utilizing TaqMan primers and reagents as outlined by the manufacturer. (ThermoFisher Scientific, Waltham, MA; GAPDH: Mm99999915\_g1, ACTB: Mm02619580\_g1, MMP13: Mm00439491\_m1, IL6: Mm00446190\_m1). GAPDH and Actin B were both used for normalizing MMP13 expression.

### In vitro matrix binding, reverse transfection in ATDC5 cells.

To select the correct polymer/antibody ratio (Fig. 2f), trypsin-damaged porcine cartilage retention was assessed. First, damaged articular cartilage “model lesions” were created by partial trypsin damage of porcine cartilage with 2.5% trypsin for 15 min at 37 °C. Then, each plug was inserted into a well plate and treated with mAbCII-siNPs or controls. The different mAbCII-siNP formulations were tested at matched polymer and siRNA concentration in the test solutions. In the screened samples, the final antibody concentrations tested were 0.66, 1.33, and 2.66 µM for the 20:1, 40:1, and 80:1 ratios of free polymer to mAbCII-conjugated polymer. Formulations were incubated for 1 h at 37 °C followed by washing twice with PBS (200 µL each time). IVIS imaging was used to quantify retention of the rhodamine within the siNP polymer.

In order to test substrate mediated delivery and potency of the mAbCII-siNPs, a reverse transfection assay was employed. Trypsin-damaged tissues (prepared as described) were incubated for 1 h with mAbCII-siNPs/siLuc, siNPs/siLuc, mAbCtrl-siNPs/siLuc, lipofectamine 2000/siLuc or the analogous formulations loaded with nonsilencing siNEG siRNA. Following incubation, explants were washed with PBS, and luciferase-expressing

ATDC5 cells (murine, chondrogenic) in DMEM/F12 1:1 media were seeded onto the treated cartilage for 24 h at 37 °C. In parallel samples, similar methods were used but without the wash step to help to gauge the silencing efficacy of the different formulations independent from the cartilage binding capacity. Each well was rinsed with PBS before adding luciferin-containing media (150 ug/mL) and evaluating luminescence by IVIS imaging. Following the measurement of luciferase expression, cell viability of each group was determined using the Promega CellTiter-Glo cell viability assay following Promega's standard protocol.

### ***In vivo* short-term mechanical loading PTOA model.**

C57 mice were mechanically loaded, 3 times per week for 2 weeks. The PTOA model of noninvasive repetitive joint loading was induced by subjecting the knee joints of mice (anesthetized with 3% isoflurane) to 250 cycles of compressive mechanical loading at 9 N. This procedure was repeated three times per week over a period of 2 weeks using conditions adapted from previous studies<sup>38,48</sup>. All mice were ordered from Charles River Labs (Wilmington, MA), all male, and aged either 8 weeks (short-term study) or 6 months (long-term study). Animals were housed within Vanderbilt University's rodent housing facilities in compliance with all procedures reviewed and approved by IACUC in standard conditions (18–23°C, 40–60% humidity, 12 light/12 dark light cycle). All relevant IACUC animal-use guidelines and ethical regulations were abided in animal work conducted for this study.

### **Joint pharmacokinetics.**

In-joint retention of mAbCII-siNPs was also assessed in both health mice and in PTOA mice using the 2-week mechanical loading protocol. The normal mice and mice that had been mechanically loaded 3 times per week for 2 weeks were treated with intra-articular injection of 0.5 mg/kg siRNA per knee in mAbCII-siNPs. Over the next 72 h, the amount of fluorescence remaining in the knee was measured by IVIS imaging (software: Living Image V4.4, Perkin Elmer, Waltham, MA) of the rhodamine-containing mAbCII-siNPs (Supplementary Fig. 4b; Exc/Emm: 548/570 nm). Cryosections of fluorescent mAbCII-siNPs were imaged using the Nikon Czi+ confocal microscope and analysed using Nikon NIS-Elements AR V4.30.01 (Nikon Inc., Minato City, Tokyo, JP).

### **Organ biodistribution.**

Intravital imaging was performed on mice after intraarticular injection of mAbCII-siNPs (0.5 mg/kg siRNA per knee) with and without mechanical induction of PTOA. These measurements were taken on the same mice used to verify mAbCII-siNP anchoring and retention within PTOA-affected knee joints (Fig. 3c) reduced level of biodistribution to the liver relative to mice which did not have PTOA induction. These data also confirmed the anticipated result that the liver is the primary clearance organ for the siNPs (Supplementary Fig. 5a,b).

### **mAbCII-siNP in vivo dose response and longevity studies.**

A progressive dose experiment was performed with the same two-week mechanical loading model. After two weeks of mechanical loading, the joints were treated, and 72 h later

joint tissues were harvested for MMP13 and IL-1 $\beta$  expression analysis by TaqMan qPCR (Supplementary Fig. 6a,b). Using the 0.5 mg/kg per knee dose, a longevity of action study was performed by intraarticular administration of mAbCII-siNPs after two weeks of mechanical loading. Mechanical loading continued with the same frequency to maintain elevated MMP13 expression in the joints, and the mice were sacrificed at 5, 10, and 15 days after injection for gene expression analysis (Supplementary Fig. 6c).

### **In vivo long-term mechanical loading therapeutic PTOA model.**

Mice were aged to 6 months and then subjected to a more rigorous cyclic mechanical loading protocol of 9 N, 500 cycles, 5 times per week, for 6 weeks<sup>49</sup>. Doses of siRNA (0.5 mg/kg) were administered into each knee weekly, starting concurrently with mechanical loading. MMPsense and Alexafluor-labeled free mAbCII antibody were injected intravenously 24 h before sacrifice to gauge total MMP activity and quantify cartilage damage, respectively.

For the clinical standard benchmarking study, a relatively high methylprednisolone dose in rodents of 4 mg/kg was administered by intraarticular injection. Separate cohorts of mice were delivered either a single treatment at the beginning of the 6-week time course or weekly treatment. Weekly treatment matched the mAbCII-siNP treatment protocol, while a single treatment was used to match the clinical standard, as patients are not typically treated more frequently than that with intraarticular steroid injections<sup>81,82</sup>. The dose was prepared by initially dissolving in DMSO, diluting in water, and injecting at a volume of 20  $\mu$ L per knee<sup>77</sup>.

### **Bone Analysis by microCT.**

All microCT analysis was performed with the ScanCo  $\mu$ CT-50 and ScanCo software V6.0 (Scanco USA, Inc., Southeastern, PA). 3D renderings were shown at a consistent density threshold (42.0% of maximum bone density, or 420 per mille). All samples were fixed with formalin and then emerged in 100% ethanol during micro-CT imaging. The scans were collected with 20  $\mu$ m thick slices, an isotropic 12  $\mu$ m voxel size, a current/voltage of 114 mA/70kVp, and an integration time of 200 millisecond. Imaging, contouring, and all sample measurements and analysis were performed on deidentified samples by a treatment-blinded user.

### **Histology and Immunohistochemistry.**

Stifles were fixed in 10% neutral buffered formalin and decalcified in Immunocal (StatLab, McKinney, TX). Tissue handling for histopathology was primarily performed in the Vanderbilt Translational Pathology Shared Resource (TPSR) by certified histotechnicians. Fixed tissues were routinely processed using a standard 8 h cycle of graded alcohols, xylenes, and paraffin wax, embedded and sectioned at 5 microns, floated on a water bath, and mounted on positively charged glass slides. Hematoxylin and eosin (H&E) staining was performed on the Gemini autostainer (Thermo Fisher Scientific, Waltham, MA). Safranin O staining was performed by hand using a kit (StatLab).

Stifle joints were evaluated by H&E and safranin O in at least 2 serial mid-frontal sections. This histopathologic interpretation was conducted by a board-certified veterinary pathologist under treatment-blinded conditions<sup>83</sup>. OARSI scores (0–6 semiquantitative scale) were provided for the medial tibial plateau and lateral tibial plateau<sup>55</sup>. Simultaneously, a generic score (0–4 semiquantitative scale) was assigned based on safranin O staining of the tibial plateau (Supplementary Table 2a) and on H&E features of degenerative joint disease (DJD) severity, as defined by cartilage degeneration, meniscal metaplasia, subchondral osteosclerosis, synovial hyperplasia and inflammation, and osteophyte/meniscal mineral deposit formation (Supplementary Table 2b)<sup>84</sup>.

Immunohistochemical staining was performed on a Leica Bond-Max autostainer (Leica Biosystems Inc., Buffalo Grove, IL). All steps besides dehydration, clearing, and coverslipping were performed on the Bond-Max where all the slides were deparaffinized. Heat-induced antigen retrieval was performed on the Bond-Max using Epitope Retrieval 1 solution (Leica Biosystems Inc.) for 20 minutes. Slides were incubated with anti-MMP13 (cat# Ab39012, Abcam, Cambridge, MA) for 1 hour at a 1:750 dilution. The Bond Polymer Refine detection system (Leica Biosystems Inc.) was used for visualization. Slides were then dehydrated, cleared, and cover slipped.

#### **nanoString inflammation panel gene expression analysis.**

The Vanderbilt Technologies for Advanced Genomics (VANTAGE) core processed the RNA (>50 ng purified, normalized RNA per sample) isolated from articular cartilage and meniscal/synovial tissue processed in equal masses. Samples were subjected to VANTAGE core quality control measures before processing using the nanoString nCounter Inflammation (mouse, V2) panel. All hybridizations were incubated for 20 hours, following manufacturer (Nanostring Technologies, Inc., Seattle, WA) recommended procedures. The nSolver V3.0 software package (Nanostring Technologies, Inc., Seattle, WA) was used for comparisons, unsupervised analysis, and gene cluster analysis between groups. Raw data and normalized data are available in Gene Expression Omnibus (accession: GSE171031; <https://www.ncbi.nlm.nih.gov/geo/query/acc.cgi?acc=GSE171031>)).

#### **Statistical analysis.**

All statistical analysis was performed as described in figure captions with GraphPad Prism V8.2 (GraphPad, San Diego, CA), except for nanoString data analysis with nSolver V3.0 (Nanostring Technologies, Inc., Seattle, WA).

#### **Reporting summary.**

Further information on research design is available in the Nature Research Reporting Summary linked to this article.

#### **Data availability**

The main data supporting the results in this study are available within the paper and its Supplementary Information. Raw and normalized nanoString datasets are available within the Gene Expression Omnibus with the accession identifier GSE171031 (<https://www.ncbi.nlm.nih.gov/geo/query/acc.cgi?acc=GSE171031>). The remaining raw and

analysed datasets from the study are too large to be publicly shared, yet they are available for research purposes from the corresponding author on reasonable request.

## Supplementary Material

Refer to Web version on PubMed Central for supplementary material.

## Acknowledgements

The authors acknowledge the assistance of the Vanderbilt Translational Pathology Shared Resource (TPSR). TPSR is supported by NCI/NIH Cancer Center Support Grant 2P30 CA068485-14. Dynamic light scattering was conducted at the Vanderbilt Institute of Nanoscale Sciences and Engineering. Bone analysis by microCT was supported in part by the NIH (S10RR027631-01). The technical assistance of Carrie B. Wiese, Joshua R Johnson, and Ray Mernaugh is also acknowledged. Vanderbilt Technologies for Advanced Genomics (VANTAGE) core performed nanoString QC and hybridization, and is supported by the Vanderbilt Ingram Cancer Center (P30 CA68485), the Vanderbilt Vision Center (P30 EY08126), and NIH/NCRR (G20 RR030956).

We are grateful to the DOD (DOD CDMRP OR130302), NIH (NIH R01 CA224241, NIH R01 EB019409), NIH (NIGMS T32GM007347), the VA Merit Award BX004151, the National Science Foundation Graduate Research Fellowship Program (NSF GRF #2016212929), the Natural Sciences and Engineering Research Council of Canada (NSERC), and the Rheumatology Research Foundation (RRF) for support.

## References

- Loeser RF Osteoarthritis year in review 2013: biology. *Osteoarthritis and Cartilage* 21, 1436–1442, doi:10.1016/j.joca.2013.05.020 (2013). [PubMed: 23774472]
- Tanamas S. et al. Does knee malalignment increase the risk of development and progression of knee osteoarthritis? A systematic review. *Arthritis Care & Research* 61, 459–467, doi:10.1002/art.24336 (2009). [PubMed: 19333985]
- Richette P. et al. Benefits of massive weight loss on symptoms, systemic inflammation and cartilage turnover in obese patients with knee osteoarthritis. *Annals of the Rheumatic Diseases* 70, 139–144, doi:10.1136/ard.2010.134015 (2011). [PubMed: 20980288]
- Valdes AM & Spector TD Genetic epidemiology of hip and knee osteoarthritis. *Nat Rev Rheumatol* 7, 23–32 (2011). [PubMed: 21079645]
- Issa S. & Sharma L. Epidemiology of osteoarthritis: An update. *Curr Rheumatol Rep* 8, 7–15, doi:10.1007/s11926-006-0019-1 (2006). [PubMed: 16515759]
- Lee AS et al. A current review of molecular mechanisms regarding osteoarthritis and pain. *Gene* 527, 440–447, doi:10.1016/j.gene.2013.05.069 (2013). [PubMed: 23830938]
- Zhang Y. & Jordan JM Epidemiology of Osteoarthritis. *Clinics in geriatric medicine* 26, 355–369, doi:10.1016/j.cger.2010.03.001 (2010). [PubMed: 20699159]
- Brophy RH, Gray BL, Nunley RM, Barrack RL & Clohisey JC Total Knee Arthroplasty After Previous Knee Surgery. *J. Bone Joint Surg.-Am Vol.* 96A, 801–805, doi:10.2106/jbjs.m.00105 (2014).
- Brown TD, Johnston RC, Saltzman CL, Marsh JL & Buckwalter JA Posttraumatic osteoarthritis: a first estimate of incidence, prevalence, and burden of disease. *Journal of orthopaedic trauma* 20, 739–744 (2006). [PubMed: 17106388]
- Young IC et al. A novel compressive stress-based osteoarthritis-like chondrocyte system. *Exp Biol Med (Maywood)* 242, 1062–1071, doi:10.1177/1535370217699534 (2017). [PubMed: 28492349]
- Martin J. & Buckwalter J. Post-traumatic osteoarthritis: the role of stress induced chondrocyte damage. *Biorheology* 43, 517–521 (2006). [PubMed: 16912423]
- McAlindon TE et al. OARSI guidelines for the non-surgical management of knee osteoarthritis. *Osteoarthritis Cartilage* 22, 363–388, doi:10.1016/j.joca.2014.01.003 (2014). [PubMed: 24462672]
- McAlindon TE et al. Effect of Intra-articular Triamcinolone vs Saline on Knee Cartilage Volume and Pain in Patients With Knee Osteoarthritis: A Randomized Clinical Trial. *JAMA* 317, 1967–1975, doi:10.1001/jama.2017.5283 (2017). [PubMed: 28510679]

14. Wijn SRW, Rovers MM, van Tienen TG & Hannink G. Intra-articular corticosteroid injections increase the risk of requiring knee arthroplasty. *Bone Joint J* 102-B, 586–592, doi:10.1302/0301-620X.102B5.BJJ-2019-1376.R1 (2020). [PubMed: 32349592]
15. Wernecke C, Braun HJ & Dragoo JL The Effect of Intra-articular Corticosteroids on Articular Cartilage: A Systematic Review. *Orthop J Sports Med* 3, 2325967115581163, doi:10.1177/2325967115581163 (2015).
16. Wang M. et al. MMP13 is a critical target gene during the progression of osteoarthritis. *Arthritis Res Ther* 15, R5, doi:10.1186/ar4133 (2013). [PubMed: 23298463]
17. Krzeski P. et al. Development of musculoskeletal toxicity without clear benefit after administration of PG-116800, a matrix metalloproteinase inhibitor, to patients with knee osteoarthritis: a randomized, 12-month, double-blind, placebo-controlled study. *Arthritis Res Ther* 9, R109, doi:10.1186/ar2315 (2007). [PubMed: 17958901]
18. Molina JR et al. A phase I and pharmacokinetic study of the selective, non-peptidic inhibitor of matrix metalloproteinase BAY 12–9566 in combination with etoposide and carboplatin. *Anticancer Drugs* 16, 997–1002 (2005). [PubMed: 16162976]
19. Clutterbuck AL, Asplin KE, Harris P, Allaway D. & Mobasheri A. Targeting matrix metalloproteinases in inflammatory conditions. *Curr Drug Targets* 10, 1245–1254 (2009). [PubMed: 19909233]
20. Liu J. & Khalil RA Matrix Metalloproteinase Inhibitors as Investigational and Therapeutic Tools in Unrestrained Tissue Remodeling and Pathological Disorders. *Prog Mol Biol Transl Sci* 148, 355–420, doi:10.1016/bs.pmbts.2017.04.003 (2017). [PubMed: 28662828]
21. Settle S. et al. Cartilage degradation biomarkers predict efficacy of a novel, highly selective matrix metalloproteinase 13 inhibitor in a dog model of osteoarthritis: confirmation by multivariate analysis that modulation of type II collagen and aggrecan degradation peptides parallels pathologic changes. *Arthritis Rheum* 62, 3006–3015, doi:10.1002/art.27596 (2010). [PubMed: 20533541]
22. Cai H. et al. Assessment of the renal toxicity of novel anti-inflammatory compounds using cynomolgus monkey and human kidney cells. *Toxicology* 258, 56–63, doi:10.1016/j.tox.2009.01.006 (2009). [PubMed: 19378467]
23. Sterner B. et al. The effect of polymer size and charge of molecules on permeation through synovial membrane and accumulation in hyaline articular cartilage. *Eur J Pharm Biopharm* 101, 126–136, doi:10.1016/j.ejpb.2016.02.004 (2016). [PubMed: 26876928]
24. Larsen C. et al. Intra-articular depot formulation principles: Role in the management of postoperative pain and arthritic disorders. *Journal of pharmaceutical sciences* 97, 4622–4654 (2008). [PubMed: 18306275]
25. Evans CH, Kraus VB & Setton LA Progress in intra-articular therapy. *Nature Reviews Rheumatology* 10, 11, doi:10.1038/nrrheum.2013.159 (2013). [PubMed: 24189839]
26. Simkin PA Synovial perfusion and synovial fluid solutes. *Ann Rheum Dis* 54, 424–428, doi:10.1136/ard.54.5.424 (1995). [PubMed: 7794054]
27. Rothenfluh DA, Bermudez H, O’Neil CP & Hubbell JA Biofunctional polymer nanoparticles for intra-articular targeting and retention in cartilage. *Nat Mater* 7, 248–254, doi:[http://www.nature.com/nmat/journal/v7/n3/supinfo/nmat2116\\_S1.html](http://www.nature.com/nmat/journal/v7/n3/supinfo/nmat2116_S1.html) (2008). [PubMed: 18246072]
28. Zhou F. et al. Silk fibroin-chondroitin sulfate scaffold with immuno-inhibition property for articular cartilage repair. *Acta Biomater* 63, 64–75, doi:10.1016/j.actbio.2017.09.005 (2017). [PubMed: 28890259]
29. Hayder M. et al. A Phosphorus-Based Dendrimer Targets Inflammation and Osteoclastogenesis in Experimental Arthritis. *Science Translational Medicine* 3, 81ra35, doi:10.1126/scitranslmed.3002212 (2011).
30. Chen K. & Chen X. Integrin targeted delivery of chemotherapeutics. *Theranostics* 1, 189–200 (2011). [PubMed: 21547159]
31. Hoy SM Patisiran: First Global Approval. *Drugs* 78, 1625–1631, doi:10.1007/s40265-018-0983-6 (2018). [PubMed: 30251172]
32. de Paula Brandão PR, Titze-de-Almeida SS & Titze-de-Almeida R. Leading RNA Interference Therapeutics Part 2: Silencing Delta-Aminolevulinic Acid Synthase 1, with a Focus on Givosiran. *Molecular Diagnosis & Therapy*, 1–8 (2019). [PubMed: 30411216]

33. Nelson CE et al. Balancing cationic and hydrophobic content of PEGylated siRNA polyplexes enhances endosome escape, stability, blood circulation time, and bioactivity in vivo. *ACS Nano* 7, 8870–8880, doi:10.1021/nn403325f (2013). [PubMed: 24041122]
34. Beavers KR, Nelson CE & Duvall CL MiRNA inhibition in tissue engineering and regenerative medicine. *Adv Drug Deliv Rev* 88, 123–137, doi:10.1016/j.addr.2014.12.006 (2015). [PubMed: 25553957]
35. Sarett SM et al. Hydrophobic interactions between polymeric carrier and palmitic acid-conjugated siRNA improve PEGylated polyplex stability and enhance in vivo pharmacokinetics and tumor gene silencing. *Biomaterials* 97, 122–132, doi:10.1016/j.biomaterials.2016.04.017 (2016). [PubMed: 27163624]
36. Jackson MA et al. Zwitterionic Nanocarrier Surface Chemistry Improves siRNA Tumor Delivery and Silencing Activity Relative to Polyethylene Glycol. *ACS Nano*, doi:10.1021/acsnano.7b01110 (2017).
37. Ruan MZ et al. Proteoglycan 4 expression protects against the development of osteoarthritis. *Sci Transl Med* 5, 176ra134, doi:10.1126/scitranslmed.3005409 (2013).
38. Cho H, Pinkhassik E, David V, Stuart JM & Hasty KA Detection of early cartilage damage using targeted nanosomes in a post-traumatic osteoarthritis mouse model. *Nanomedicine : nanotechnology, biology, and medicine* 11, 939–946, doi:10.1016/j.nano.2015.01.011 (2015).
39. Nelson CE et al. Balancing Cationic and Hydrophobic Content of PEGylated siRNA Polyplexes Enhances Endosome Escape, Stability, Blood Circulation Time, and Bioactivity in Vivo. *ACS Nano* 7, 8870–8880, doi:10.1021/nn403325f (2013). [PubMed: 24041122]
40. Werfel TA et al. Selective mTORC2 Inhibitor Therapeutically Blocks Breast Cancer Cell Growth and Survival. *Cancer Res* 78, 1845–1858, doi:10.1158/0008-5472.CAN-17-2388 (2018). [PubMed: 29358172]
41. Werfel TA et al. Combinatorial optimization of PEG architecture and hydrophobic content improves ternary siRNA polyplex stability, pharmacokinetics, and potency in vivo. *J Control Release* 255, 12–26, doi:10.1016/j.jconrel.2017.03.389 (2017). [PubMed: 28366646]
42. Kilchrist KV et al. Gal8 Visualization of Endosome Disruption Predicts Carrier-Mediated Biologic Drug Intracellular Bioavailability. *ACS Nano* 13, 1136–1152, doi:10.1021/acsnano.8b05482 (2019). [PubMed: 30629431]
43. Jackson MA et al. Dual carrier-cargo hydrophobization and charge ratio optimization improve the systemic circulation and safety of zwitterionic nano-polyplexes. *Biomaterials* 192, 245–259, doi:10.1016/j.biomaterials.2018.11.010 (2019). [PubMed: 30458360]
44. Jackson MA et al. Zwitterionic Nanocarrier Surface Chemistry Improves siRNA Tumor Delivery and Silencing Activity Relative to Polyethylene Glycol. *ACS Nano* 11, 5680–5696, doi:10.1021/acsnano.7b01110 (2017). [PubMed: 28548843]
45. Griffin DJ et al. Effects of enzymatic treatments on the depth-dependent viscoelastic shear properties of articular cartilage. *J Orthop Res* 32, 1652–1657, doi:10.1002/jor.22713 (2014). [PubMed: 25196502]
46. Cho H. et al. Theranostic immunoliposomes for osteoarthritis. *Nanomedicine* 10, 619–627, doi:10.1016/j.nano.2013.09.004 (2014). [PubMed: 24096032]
47. Jasin HE, Noyori K, Takagi T. & Taurog JD Characteristics of anti-type II collagen antibody binding to articular cartilage. *Arthritis Rheum* 36, 651–659, doi:10.1002/art.1780360512 (1993). [PubMed: 8489543]
48. Poulet B, Hamilton RW, Shefelbine S. & Pitsillides AA Characterizing a novel and adjustable noninvasive murine joint loading model. *Arthritis and rheumatism* 63, 137–147, doi:10.1002/art.27765 (2011). [PubMed: 20882669]
49. Ko FC et al. In vivo cyclic compression causes cartilage degeneration and subchondral bone changes in mouse tibiae. *Arthritis Rheum* 65, 1569–1578, doi:10.1002/art.37906 (2013). [PubMed: 23436303]
50. Scanzello CR & Goldring SR The role of synovitis in osteoarthritis pathogenesis. *Bone* 51, 249–257, doi:10.1016/j.bone.2012.02.012 (2012). [PubMed: 22387238]
51. Goldring MB Articular cartilage degradation in osteoarthritis. *HSS J* 8, 7–9, doi:10.1007/s11420-011-9250-z (2012). [PubMed: 23372517]

52. Glasson SS, Chambers MG, Van Den Berg WB & Little CB The OARSI histopathology initiative – recommendations for histological assessments of osteoarthritis in the mouse. *Osteoarthritis and Cartilage* 18, S17–S23, doi:10.1016/j.joca.2010.05.025 (2010).
53. Eichaker LR, Cho H, Duvall CL, Werfel TA & Hasty KA Future nanomedicine for the diagnosis and treatment of osteoarthritis. *Nanomedicine* 9, 2203–2215, doi:10.2217/nmm.14.138 (2014). [PubMed: 25405797]
54. O’Grady KP et al. Drug-Free ROS Sponge Polymeric Microspheres Reduce Tissue Damage from Ischemic and Mechanical Injury. *ACS Biomaterials Science & Engineering*, doi:10.1021/acsbiomaterials.6b00804 (2017).
55. Glasson SS, Chambers MG, Van Den Berg WB & Little CB The OARSI histopathology initiative - recommendations for histological assessments of osteoarthritis in the mouse. *Osteoarthritis Cartilage* 18 Suppl 3, S17–23, doi:10.1016/j.joca.2010.05.025 (2010).
56. Sun Y. & Mauerhan DR Meniscal calcification, pathogenesis and implications. *Current opinion in rheumatology* 24, 152–157 (2012). [PubMed: 22227878]
57. Blom AB et al. Crucial role of macrophages in matrix metalloproteinase-mediated cartilage destruction during experimental osteoarthritis: involvement of matrix metalloproteinase 3. *Arthritis and rheumatism* 56, 147–157, doi:10.1002/art.22337 (2007). [PubMed: 17195217]
58. Hügle T. & Geurts J. What drives osteoarthritis?—Synovial versus subchondral bone pathology. *Rheumatology* 56, 1461–1471 (2016).
59. Goldring SR Alterations in periarticular bone and cross talk between subchondral bone and articular cartilage in osteoarthritis. *Ther Adv Musculoskelet Dis* 4, 249–258, doi:10.1177/1759720X12437353 (2012). [PubMed: 22859924]
60. Boileau C, Tat SK, Pelletier JP, Cheng S. & Martel-Pelletier J. Diacerein inhibits the synthesis of resorptive enzymes and reduces osteoclastic differentiation/survival in osteoarthritic subchondral bone: a possible mechanism for a protective effect against subchondral bone remodelling. *Arthritis Res Ther* 10, R71, doi:10.1186/ar2444 (2008). [PubMed: 18578867]
61. Punzi L. et al. Post-traumatic arthritis: overview on pathogenic mechanisms and role of inflammation. *RMD Open* 2, e000279, doi:10.1136/rmdopen-2016-000279 (2016).
62. Christiansen BA et al. Non-invasive mouse models of post-traumatic osteoarthritis. *Osteoarthritis Cartilage* 23, 1627–1638, doi:10.1016/j.joca.2015.05.009 (2015). [PubMed: 26003950]
63. Almasry SM, Soliman HM, El-Tarhouny SA, Algaidi SA & Ragab EM Platelet rich plasma enhances the immunohistochemical expression of platelet derived growth factor and vascular endothelial growth factor in the synovium of the meniscectomized rat models of osteoarthritis. *Ann Anat* 197, 38–49, doi:10.1016/j.aanat.2014.10.006 (2015). [PubMed: 25466931]
64. Solomon LA, Bérubé NG & Beier F. Transcriptional regulators of chondrocyte hypertrophy. *Birth Defects Res C Embryo Today* 84, 123–130, doi:10.1002/bdrc.20124 (2008). [PubMed: 18546336]
65. Zhai G, Doré J. & Rahman P. TGF- $\beta$  signal transduction pathways and osteoarthritis. *Rheumatol Int* 35, 1283–1292, doi:10.1007/s00296-015-3251-z (2015). [PubMed: 25773660]
66. Shen J, Li S. & Chen D. TGF- $\beta$  signaling and the development of osteoarthritis. *Bone Res* 2, doi:10.1038/boneres.2014.2 (2014).
67. Lee YH et al. Enzyme-crosslinked gene-activated matrix for the induction of mesenchymal stem cells in osteochondral tissue regeneration. *Acta Biomater* 63, 210–226, doi:10.1016/j.actbio.2017.09.008 (2017). [PubMed: 28899816]
68. John T, Stahel PF, Morgan SJ & Schulze-Tanzil G. Impact of the complement cascade on posttraumatic cartilage inflammation and degradation. *Histol Histopathol* 22, 781–790, doi:10.14670/HH-22.781 (2007). [PubMed: 17455152]
69. Silawal S, Triebel J, Bertsch T. & Schulze-Tanzil G. Osteoarthritis and the Complement Cascade. *Clin Med Insights Arthritis Musculoskelet Disord* 11, 1179544117751430, doi:10.1177/1179544117751430 (2018).
70. Lubbers R, van Essen MF, van Kooten C. & Trouw LA Production of complement components by cells of the immune system. *Clin Exp Immunol* 188, 183–194, doi:10.1111/cei.12952 (2017). [PubMed: 28249350]

71. Takahashi N. et al. Elucidation of IL-1/TGF-beta interactions in mouse chondrocyte cell line by genome-wide gene expression. *Osteoarthritis Cartilage* 13, 426–438, doi:10.1016/j.joca.2004.12.010 (2005). [PubMed: 15882566]
72. Klein-Wieringa IR et al. Inflammatory Cells in Patients with Endstage Knee Osteoarthritis: A Comparison between the Synovium and the Infrapatellar Fat Pad. *The Journal of rheumatology* 43, 771–778, doi:10.3899/jrheum.151068 (2016). [PubMed: 26980579]
73. Wu CL, Harasymowicz NS, Klimak MA, Collins KH & Guilak F. The Role of Macrophages in Osteoarthritis and Cartilage Repair. *Osteoarthritis Cartilage*, doi:10.1016/j.joca.2019.12.007 (2020).
74. Mazur CM et al. Osteocyte dysfunction promotes osteoarthritis through MMP13-dependent suppression of subchondral bone homeostasis. *Bone Res* 7, 34, doi:10.1038/s41413-019-0070-y (2019). [PubMed: 31700695]
75. Goldring SR & Goldring MB in Kelley's textbook of rheumatology 1–19. e16 (Elsevier, 2017).
76. Garg N, Perry L. & Deodhar A. Intra-articular and soft tissue injections, a systematic review of relative efficacy of various corticosteroids. *Clinical rheumatology* 33, 1695–1706 (2014). [PubMed: 24651914]
77. Cho H, Walker A, Williams J. & Hasty KA Study of osteoarthritis treatment with anti-inflammatory drugs: cyclooxygenase-2 inhibitor and steroids. *Biomed Res Int* 2015, 595273, doi:10.1155/2015/595273 (2015).
78. Hoshyar N, Gray S, Han H. & Bao G. The effect of nanoparticle size on in vivo pharmacokinetics and cellular interaction. *Nanomedicine (Lond)* 11, 673–692, doi:10.2217/nmm.16.5 (2016). [PubMed: 27003448]
79. Terato K. et al. Induction of arthritis with monoclonal antibodies to collagen. *J Immunol* 148, 2103–2108 (1992). [PubMed: 1545120]
80. Evans BC et al. Ex Vivo Red Blood Cell Hemolysis Assay for the Evaluation of pH-responsive Endosomolytic Agents for Cytosolic Delivery of Biomacromolecular Drugs. *Journal of Visualized Experiments : JoVE*, 50166, doi:10.3791/50166 (2013).
81. Polderman JA et al. Adverse side effects of dexamethasone in surgical patients. *Cochrane Database Syst Rev* 11, CD011940, doi:10.1002/14651858.CD011940.pub3 (2018).
82. Orak MM et al. Comparison of the effects of chronic intra-articular administration of tenoxicam, diclofenac, and methylprednisolone in healthy rats. *Acta Orthop Traumatol Turc* 49, 438–446 (2015). [PubMed: 26312474]
83. Bolon B. et al. Rodent preclinical models for developing novel antiarthritic molecules: comparative biology and preferred methods for evaluating efficacy. *J Biomed Biotechnol* 2011, 569068, doi:10.1155/2011/569068 (2011).
84. Aigner T. & Söder S. Histopathologische Begutachtung der Gelenkdegeneration. *Der Pathologe* 27, 431–438, doi:10.1007/s00292-006-0864-8 (2006). [PubMed: 17041774]

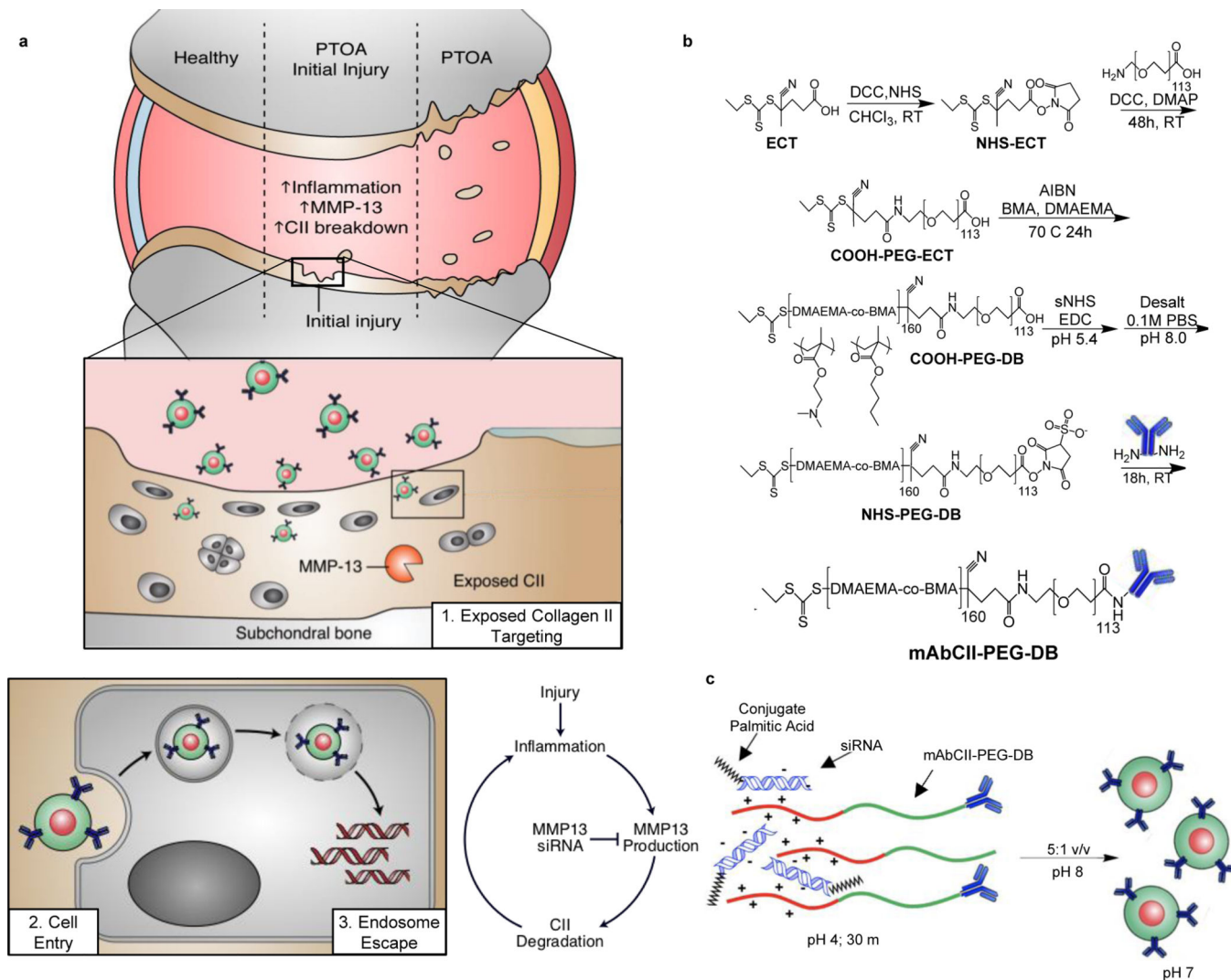


**Fig. 1 |. Synthesis of mAbCII-siNPs.**

**a.** The top left schematic illustrates the progression (left to right) from healthy knee joint, through inflammation induction following traumatic injury, to cartilage loss and degenerative joint disease (including synovial response). Degradation of cartilage enhances inflammation, inducing a degenerative cycle (lower right). The center and lower left graphics illustrate the concept of the matrix targeted nanocarriers for enhanced retention and intracellular activity of siRNA at sites of cartilage injury. **b.** Polymer synthesis and mAbCII conjugation scheme (RT: room temperature; -DB: Poly(DMAEMA-co-BMA); DCC: N,N'-Dicyclohexylcarbodiimide; DMAP: 4-dimethylaminopyridine; AIBN: azobisisobutyronitrile); **c.** Formulation schematic for siRNA cargo loading and assembly of mAbCII-siNPs. First, the polymer is dissolved in a pH 4 solution (to protonate DMAEMA making it more positively charged). This solution is then mixed with the negatively charged siRNA (with lipid tail to interact better with BMA component of polymer) for 30 mins to allow electrostatic siRNA complexation by the polymer. Next, a 5:1 v/v of pH 8 buffer is added dropwise to adjust the solution to physiologic pH of 7.4. Red = cationic and

endosomolytic DB component of polymer, green = colloiddally stabilizing poly(ethylene glycol) (PEG) component of polymer, blue = mAbCII monoclonal antibody.

Author Manuscript

Author Manuscript

Author Manuscript

Author Manuscript

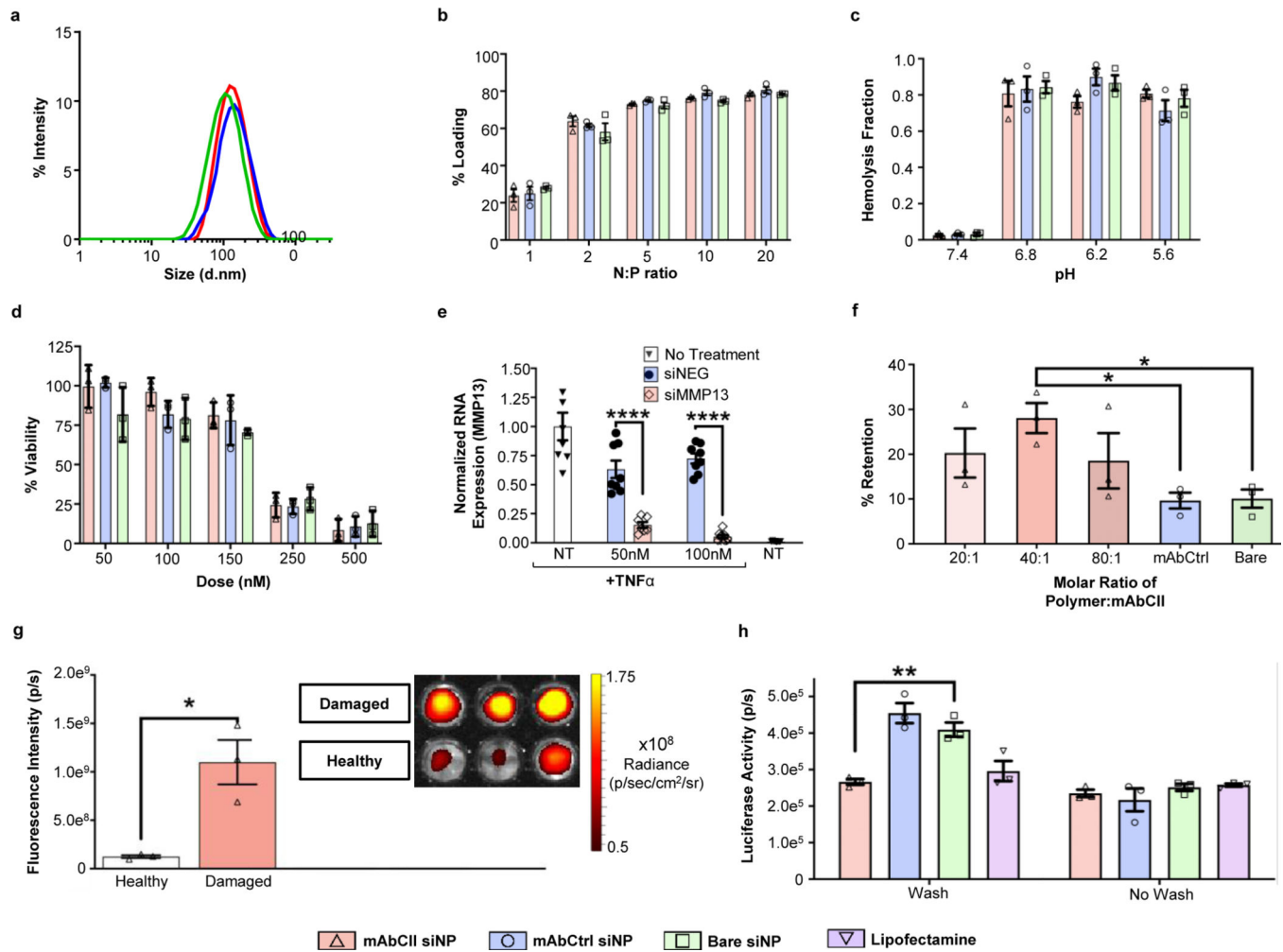


**Fig. 2 |. In vitro chemico-physical, gene silencing, and cartilage retention characterization of mAbCII-siNPs relative to bare and mAbCtrl-functionalized siNPs.**

**a.** siNP sizing by dynamic light scattering (DLS); **b.** siRNA encapsulation by Ribogreen assay ( $n=3$  technical replicates) where N:P is the ratio of positive nitrogen groups, N+, in polymer side chains to negative phosphate groups, P-, in the siRNA cargo backbone; (% calculation based on Ribogreen fluorescence of free siRNA at the same concentration); **c.** pH-triggered membrane disruption by hemolysis assay ( $n=3$  technical replicates); **d.** Dose-dependent cytocompatibility of siNPs in ATDC5 cells ( $n=3$  biological replicates) as measured using the Promega CellTiter-Glo® Luminescent Cell Viability Assay (% calculation based on luminescence of untreated cells cultured in parallel in otherwise equivalent conditions); **e.** MMP13 silencing by mAbCII-siNPs in ATDC5 cells stimulated with TNF $\alpha$  [siMMP13 vs siNEG 50nM and 100nM:  $p<0.0001$ ; one-way ANOVA, followed by a Tukey's test for multiple comparisons ( $\alpha=0.05$ );  $n=7-9$  biological replicates ( $n=7$  untreated groups with and without TNF $\alpha$ ,  $n=9$  for treated groups); gene expression normalized to that of untreated, TNF $\alpha$ -stimulated cells]; **f.** Retention of siNPs (as measured by IVIS imaging of polymer rhodamine fluorescence) with varied polymer:mAbCII molar ratios on trypsin-damaged porcine cartilage explants (40:1 mAbCII-siNP vs Bare-siNP:  $p=0.039$ , 40:1 mAbCII-siNP vs mAbCtrl siNP:  $p=0.034$ ; one-way ANOVA, followed

by a Dunnett's test for multiple comparisons ( $\alpha=0.05$ );  $n=3$  cartilage explant biological replicates; % calculation based on the fluorescence of the fluorescence of cartilage samples after treatment media removal but before washing); **g.** Retention of mAbCII-siNPs on healthy and trypsin-damaged porcine cartilage explants (as measured by intravital IVIS imaging of polymer fluorescence, rhodamine); area ( $\text{cm}^2$ ) and steradian (sr) remained constant between all measurements (Healthy vs Damaged:  $p=0.0132$ ; all samples pictured from technical replicates; unpaired two-sided t-test); **h.** Substrate-mediated gene silencing of MMP13 *in vitro* is enhanced by mAbCII-siNP binding and retention on trypsin-damaged porcine cartilage; one-way ANOVA, followed by a Tukey's test for multiple comparisons ( $\alpha=0.05$ ); (mAbCII-siNP vs Bare-siNP:  $p=0.008$ ;  $n=3$  cartilage explant biological replicates; area ( $\text{cm}^2$ ) and steradian (sr) remained constant between all measurements; \* =  $p < 0.05$ ; \*\* =  $p < 0.01$ ; \*\*\* =  $p < 0.001$ , \*\*\*\* =  $p < 0.0001$ ; center values: mean; error bars: s.e.).

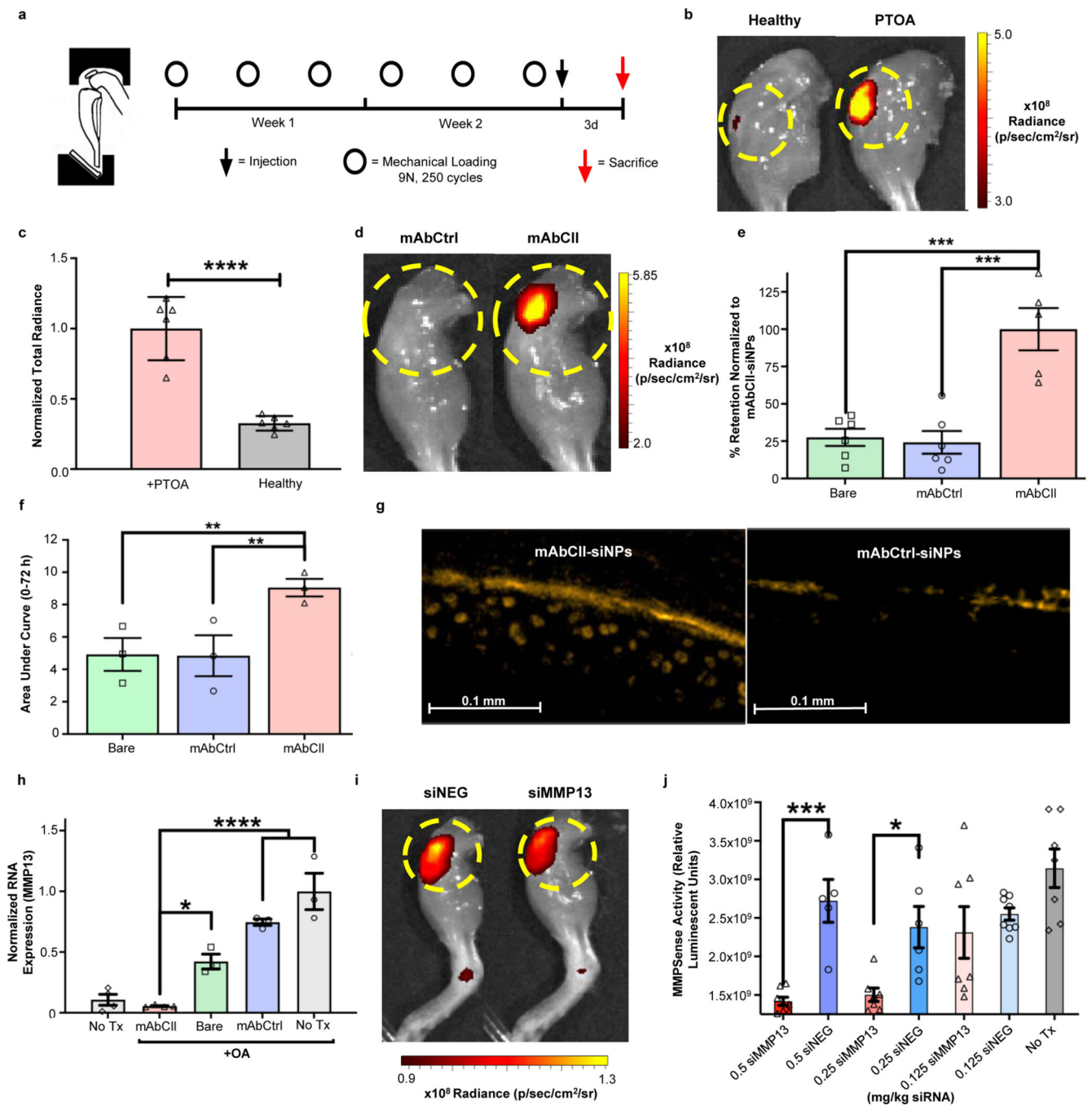


**Fig. 3 | mAbCII-siNP/siMMP13 are locally-retained and potently silence MMP13 relative to bare and mAbCtrl-functionalized siNPs in the knee joints of a short-term mouse model of PTOA.**

**a.** Schematic of the mouse knee mechanical loading apparatus (TA instruments ElectroForce 3100 with a custom 3D printed fitting for the mouse knee and for the ankle/leg) with the corresponding loading regimen used in the short-term PTOA model studies; **b-c.** Intravital imaging (**b**) and quantification (**c**) of mAbCII-siNP retention in healthy versus PTOA knee joints (Yellow dashed circles represent area of quantified fluorescence; Fluorescence normalized to background signal in PTOA joints with no treatment; PTOA vs Healthy:

p<0.0001; n=6 knees as biological replicates); **d-e**. Representative *ex vivo* imaging (**d**) and quantification (**e**) of retention of mAbCII-siNPs compared to mAbCtrl- and Bare-siNPs in PTOA knee joints explanted at 3 days (Yellow dashed circles represent area of quantified fluorescence; mAbCII-siNP vs Bare-siNP: p=0.0002, vs mAbCtrl: p=0.0001; mAbCII-siNP: n=5, other groups: n=6 mice knee joints as biological replicates); **f**. *In vivo* PTOA knee joint retention of bare, mAbCII- and mAbCtrl-siNPs presented as pharmacokinetic area under the curve (AUC) calculated from intravital imaging over 3 days post-treatment (mAbCII-siNP vs Bare-siNP: p=0.003, vs mAbCtrl siNP: p=0.003; n=3 mice); **g**. Cartilage penetration and retention of mAbCII-siNPs vs mAbCtrl-siNPs 12 hours after injection into PTOA knee joints tracked by rhodamine-labeled siNPs (pictured as orange); representative image was selected from 3 different knee joint samples, based on quality/intactness of tissue cryosection; **h**. *In vivo* gene expression of MMP13 measured by TaqMan qPCR in mouse knees treated with 0.5 mg/kg siRNA dose per knee using mAbCII, mAbCtrl, or bare siNPs [mAbCII-siNP vs Bare-siNP: p=0.012, vs mAbCtrl-siNP and No Tx (No Treatment) with PTOA: p<0.0001; n=3–4 mice knee joints as biological replicates; RNA expression normalized to untreated, PTOA]; **i-j**. Representative images of total MMP activity as visualized with MMPsense probe at 0.5 mg/kg siRNA dose (**i**) and total MMP activity quantified for varied siRNA doses (**j**) (Yellow dashed circles represent area of quantified fluorescence; siMMP13 vs siNEG 0.5mg/kg: p=0.0008, 0.25mg/kg: p=0.027; n=5–8 mice knee joints as biological replicates; varied n of progressive dose groups from failed injections disqualified at time of injection; \* = p < 0.05; \*\* = p < 0.01; \*\*\* = p < 0.001; (c, j) unpaired, two-sided t-tests; (e,f,h) one-way ANOVA, followed by a Tukey's test for multiple comparisons ( $\alpha=0.05$ ); center values: mean; error bars: s.e.).

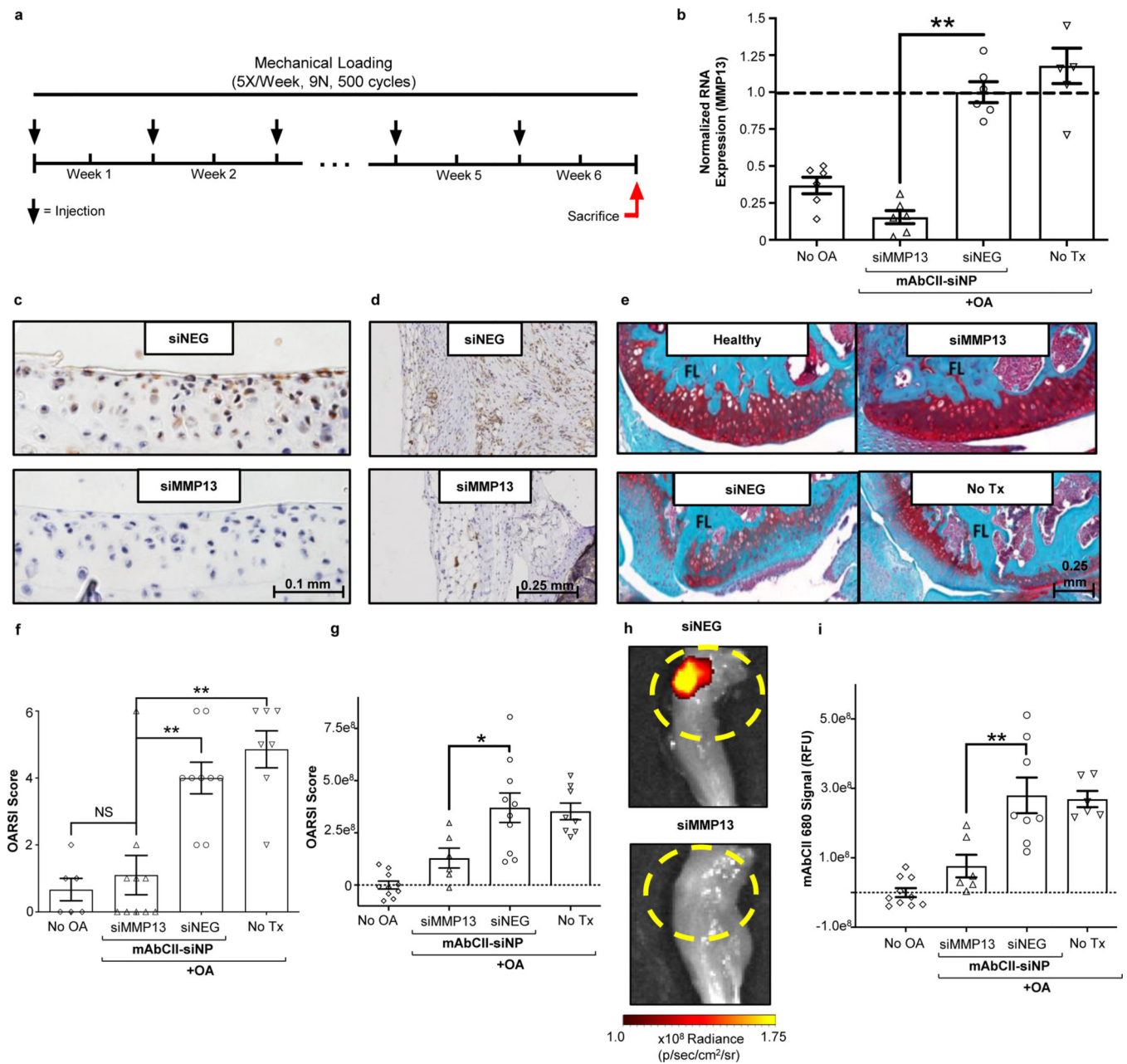


**Fig. 4 | Long-term MMP13 silencing reduces MMP13 protein levels in cartilage and synovium and protects mechanically-loaded joints from OA progression.**

**a.** Loading and treatment regimen used in the long-term PTOA mouse model; **b.** MMP13 expression at the end of week 6 (siMMP13 vs siNEG:  $p < 0.0001$ ;  $n = 5-6$  mice knee joints as biological replicates; RNA expression normalized to the average of the siNEG-treated PTOA joints); **c.** Immunohistochemical staining of MMP13+ regions (brown) of the tibial articular cartilage treated with siNEG (top) and showing reduced MMP13 protein levels when treated with mAbCII-siNPs/siMMP13 (bottom); **d.** Immunohistochemical staining of MMP13+ regions (brown) of the synovial tissue treated with siNEG (top) and showing reduced MMP13 protein levels when treated with mAbCII-siNPs/siMMP13 (bottom); for

(c-d: representative images taken from images on 3 independent samples based on the most intact tissue section for each group); **e**. Representative Safranin O staining of the articular surface of the femur in healthy mice (top left), and PTOA mice treated with siMMP13 (top right), siNEG (bottom left) and no treatment (bottom right); **f**. Quantification of cartilage damage by the OARSI osteoarthritis cartilage histopathology assessment system (e,f: siMMP13 vs No OA:  $p=0.99$ , vs siNEG:  $p=0.001$ , vs No Tx:  $p<0.0001$ ;  $n=6-9$  mice knee joints as biological replicates with each replicate imaged); **g**. Total MMP activity at 6 weeks measured by MMPsense probe, normalized to mean MMPsense fluorescence average in healthy knees without PTOA; siMMP13 vs siNEG:  $p=0.016$ ;  $n=6-10$  mice knee joints as biological replicates; **h-i**. Representative images (**h**) and quantification (**i**) of the binding of fluorescently labeled mAbCII in the knee joint at 6 weeks as a marker for relative cartilage damage and resultant exposure of CII (siMMP13 vs siNEG:  $p=0.002$ ;  $n=6-10$  mice knee joints as biological replicates with each replicate imaged; \* =  $p<0.05$ ; \*\* =  $p<0.01$ ; \*\*\* =  $p<0.001$ ; \*\*\*\* =  $p<0.0001$ ; varied  $n$  of progressive dose groups from failed intra-articular injections of treatment, failed tail-vein injection of mAbCII 680, or failure to retrieve adequate sections for histological scoring; (b,f,g,i) one-way ANOVA, followed by a Tukey's test for multiple comparisons ( $\alpha=0.05$ ); center values: mean; error bars: s.e.).

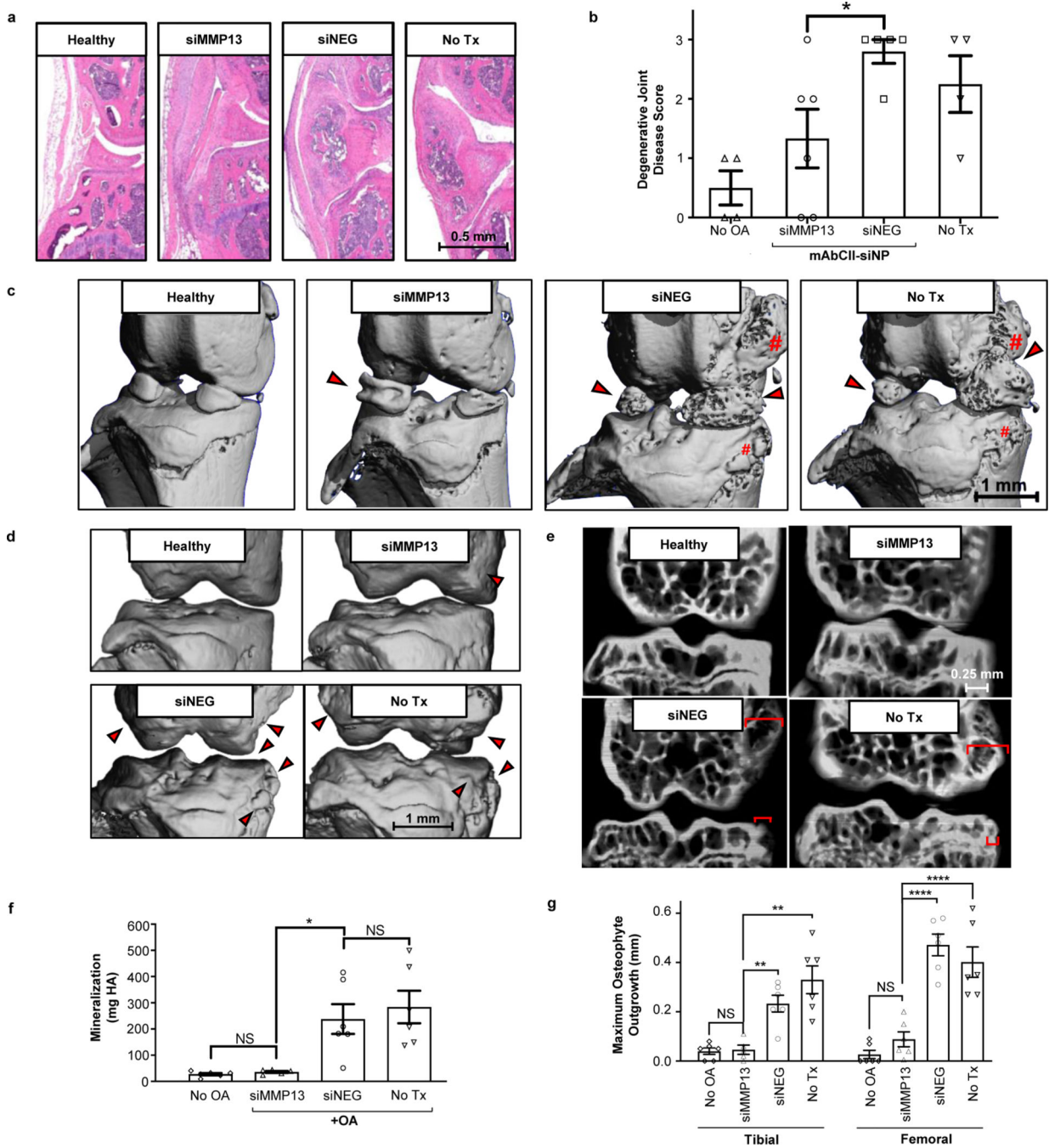


**Fig. 5 | mAbCII-siNP/siMMP13 treatment provides whole knee joint protection by reducing synovial thickening, osteophyte formation, and meniscal mineralization.**

**a-b.** Hematoxylin & Eosin (H&E) staining of knee joints, focusing on the synovial regions (a), and average Degenerative Joint Disease (DJD) Score by treatment group (b); Blinded histological scoring (using the criteria in Supplementary Item #1, Table S2) was completed by a treatment-blinded histopathologist [siMMP13 vs siNEG: p=0.042; n=4–6 mice knee joints (n=4 for healthy and untreated PTOA mice, n=5 for siNEG, n=6 for siMMP13) as biological replicates]; c. 3-dimensional (3D) microCT renderings of

meniscal/ectopic mineralization and osteophyte growth in a healthy control and PTOA mice treated with siMMP13, siNEG, and without treatment (left to right), (Arrows: meniscal/ectopic mineralization; #: Osteophyte formations); **d.** MicroCT 3D rendering of osteophytes (marked with red arrows) in a healthy control (top left) and PTOA mice treated with siMMP13 (top right), siNEG bottom left) and without treatment (bottom right); **e.** Cross-sectional microCT views used to measure osteophyte outgrowth size (red bar) in a healthy control (top left), and PTOA mice treated with siMMP13 (top right), siNEG bottom left) and without treatment (bottom right); **f.** Quantified amount of ectopic mineralization [hydroxyapatite (HA)] in the menisci and in the form of osteophytes [siMMP13 vs No OA:  $p=0.999$ , vs siNEG:  $p=0.025$ , siNEG vs No TX:  $p=0.88$ ;  $n=5-6$  mice knee joints ( $n=5$  for siMMP13,  $n=6$  for all other groups) as biological replicates]; **g.** Measurements of both tibial and femoral osteophyte size at largest outgrowth from normal cortical bone structure [Tibial: siMMP13 vs No OA:  $p=0.999$ , vs siNEG:  $p=0.005$ , siNEG vs No TX:  $p=0.25$ ; Femoral: siMMP13 vs No OA:  $p=0.72$ , vs siNEG:  $p<0.0001$ , siNEG vs No TX:  $p=0.64$ ;  $n=6$  mice knee joints as biological replicates; center values: mean; error bars: s.e.; images for parts a, c, d, and e were taken for each biological replicate; \* =  $p < 0.05$ ; \*\* =  $p < 0.01$ ; \*\*\* =  $p < 0.001$ ; \*\*\*\* =  $p < 0.0001$ ; (**b,f,g**) one-way ANOVA, followed by a Tukey's test for multiple comparisons ( $\alpha=0.05$ )]

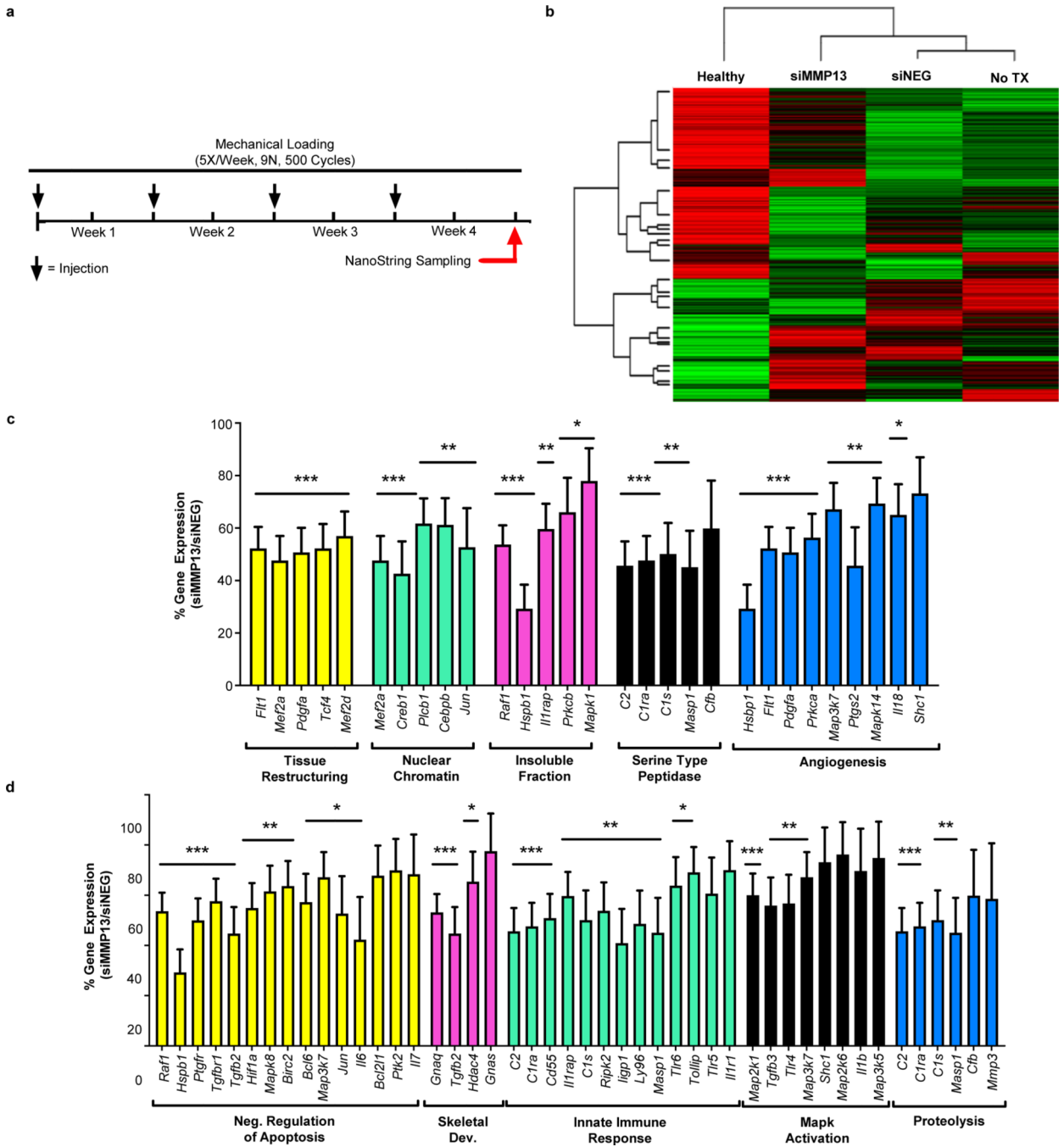


**Fig. 6 | MMP13 silencing by mAbCII-siNP/siMMP13 treatment globally impacts gene expression patterns within mechanically-loaded PTOA joints.**  
**a.** Loading and treatment regimen used for the nanoString analysis study; **b.** Unsupervised sorting of treatment groups from most to least similar to normal joints as quantified by nanoString at the end of week 4. Gene expression is shown as high- (green) or low-expression (red) sorted vertically by differences between treatment groups; **c-d.** Gene clusters were significantly different between siNEG- and siMMP13-treated joints [5 most changed in **c**, next 5 most changed in **d**; gene expression normalized to 6 internal reference

genes (CLTC, GAPDH, GUSB, HPRT, PGK1, TUBB5)]. The plots are arranged such that the clusters' p-values between siMMP13 and siNEG treatment groups is lowest on left and highest on right [n=4–8 mice knee joints (biological replicates; n=4 for healthy, n=6 untreated, n=8 for siMMP13 and siNEG) with triplicate technical measurements; statistical analysis of all groups was conducted using nanoString software to perform one-way ANOVA, followed by a Tukey's test for multiple comparisons ( $\alpha=0.05$ ); \* =  $p < 0.05$ ; \*\* =  $p < 0.01$ ; \*\*\* =  $p < 0.001$ ; center values: mean; error bars: s.e.]. The complete nanoString data set is available in the Gene Expression Omnibus: GSE171031.

Author Manuscript

Author Manuscript

Author Manuscript

Author Manuscript

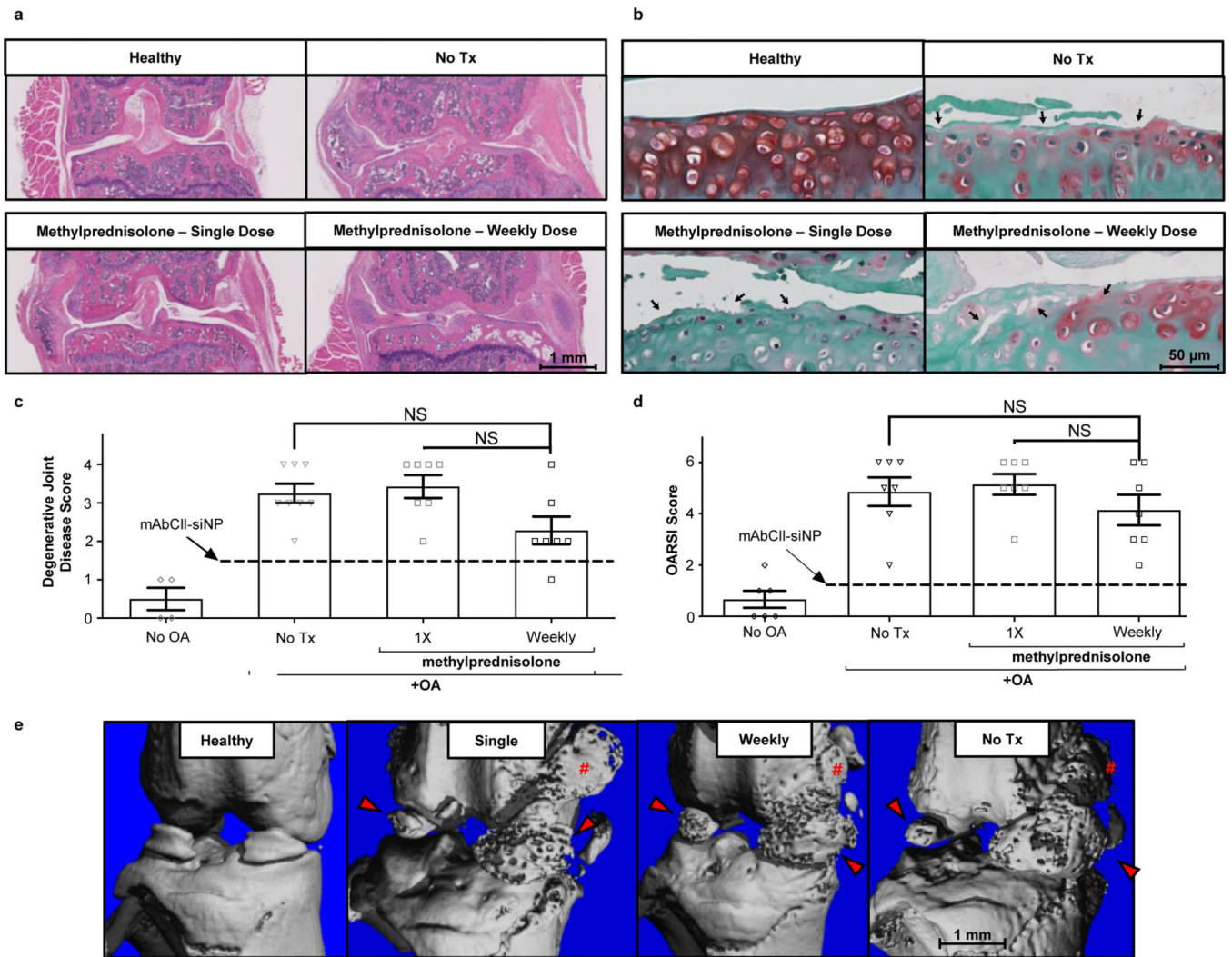


**Fig. 7 |. Clinical gold standard steroid treatment with methylprednisolone does not provide DMOAD effects in a long-term PTOA mouse model, unlike mAbCII-siNP/siMMP13 treatment.**

**a.** Representative whole joint histological sections stained with hematoxylin & eosin (H&E) after 6 weeks in a healthy control (top left), and in PTOA mice with no treatment (top right), a single dose of methylprednisolone (bottom left) and a weekly dose of methylprednisolone (bottom right); **b.** Representative safranin-O staining of the articular surface of the tibia and femur after 6 weeks in a healthy control (top left), and in PTOA mice with no treatment (top right), a single dose of methylprednisolone (bottom left), and a weekly dose of methylprednisolone (bottom right); Arrows highlight focal cartilage damage and regions of cartilage degeneration; **c.** Total joint scores by DJD were determined from H&E stained slides by a treatment-blinded histopathologist; mAbCII-siNP/siMMP13 treatment scores were overlaid for comparison (dashed line) [Weekly Prednisolone vs No Tx:  $p=0.73$ , vs Single Dose Prednisolone:  $p=0.48$ ;  $n=4-8$  mice knee joints ( $n=4$  for healthy mice,  $n=8$  for untreated PTOA mice,  $n=7$  for one-time and weekly methylprednisolone groups) as biological replicates]; **d.** Cartilage integrity was scored by the OARSI osteoarthritis cartilage histopathology assessment system by a

treatment-blinded histopathologist; mAbCII-siNP/siMMP13 treatment scores were overlaid for comparison (dashed line) [Weekly Prednisolone vs No Tx:  $p=0.11$ , vs Single Dose Prednisolone:  $p=0.057$ ;  $n=6-7$  mice knee joints ( $n=6$  for healthy mice,  $n=7$  for all other groups) as biological replicates]; **e.** MicroCT 3D reconstructions of osteophytes and ectopic mineralization in meniscus and surrounding tissues after 6 weeks in a healthy control, and in PTOA mice with a single dose of methylprednisolone, a weekly dose of methylprednisolone, and no treatment (left to right) (Arrows: meniscal mineralization; #: Osteophyte formations;  $n=3$  mice knee joints as biological replicates rendered by microCT; images for parts a, b, and e were taken for each biological replicate; (c,d) one-way ANOVA, followed by a Tukey's test for multiple comparisons ( $\alpha=0.05$ ); center values: mean; error bars: s.e.).

Author Manuscript

Author Manuscript

Author Manuscript

Author Manuscript